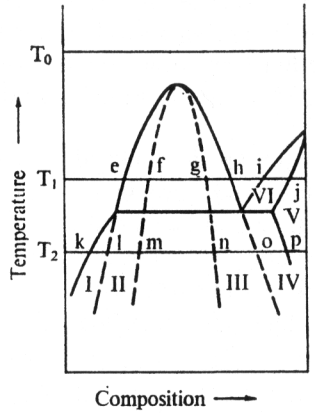


**Figure Q4-3.**

**3.** For the phase diagram shown (Fig. Q4-3), sketch the free energy vs. composition diagrams at temperatures $T_0$, $T_1$, and $T_2$. (Answer: See Cahn and Charles. Ref. 5)

## References


1. J. H. Hildebrand, *J. Am. Chem. Soc.* **51**, 66 (1929).
2. J. W. Cahn, *Trans. Met. Soc. AIME* **242**, 166–180 (1960).
3. J. W. Cahn and J. E. Hilliard, *J. Chem. Phys.* **31**(3), 688–699 (1959).
4. M. Hillert, *Acta. Met.* **9**, 525 (1961).
5. J. W. Cahn and R. J. Charles, *Phys. Chem. Glasses* **6**(5), 181–191 (1965).
6. J. E. Hilliard, in *Phase Transformations.* Ed. H. I. Aaronson, *American Society for Metals*, Metals Park, OH, (1970), ASM, 1970.
7. A. K. Varshneya, A. R. Cooper, and M. Cable, *J. Appl. Phys.* **37**(5), 2199 (1966).
8. W. Skatulla and L. Horn, *Exp. Techn. Physik* **8**, 1–9 (1960).
9. O. V. Mazurin and E. A. Porai-Koshits, Eds., *Phase Separation in Glass.* North-Holland, Amsterdam, 1984.
10. W. Vogel, *Chemistry of Glass.* Amer. Ceram. Soc., 1985.
11. See, for example, Ref. 10, p. 113; T. H. Elmer and M. E. Nordberg, *J. Am. Ceram. Soc.* **41**, 517–520 (1958); and W. Vogel, *Bull. of C.G.C.R.I. India* **2–3**, 95–107 (1975).
12. W. Vogel, W. Schmidt, and L. Horn, *Z. Chem.* **9**, 401–440 (1969).
13. A. Bhargava, A. K. Varshneya, and R. L. Snyder, *Mat. Lett.* **8**(1–2), 41–45 (1989); *Ibid.*, **11**(10–12), 313–316 (1991).


## Chapter 5

# Glass Compositions and Structures

Having looked at the glass-forming criteria and the morphological features in glasses, we will now look into the atomic configurations that are thought to be present in various glass compositions of scientific and commercial interest. It should be clearly understood that the proposed configurations are those believed generally. Occasional challenges to such beliefs do exist.

The chapter is introduced by first discussing the various ways in which glass formulae are presented. In drawing the atomic configurations, two schemes are used: (i) bonded open and solid circles with missing third dimension, and (ii) chemical symbols with the appropriate number of bonds to sketch a 2-D projection (a 'pancaked' version). The second scheme is preferred. The reader is encouraged to practice the drawing of glass network configurations: one picture is worth a thousand words!

### 5.1. Presentation of Glass Formulae

Glass formulations may be presented on a mol %, wt. %, mole fraction, mole formula, or weight fraction basis. In oxide glasses, the convention is to list the glass network modifiers in increasing valency order ending with glass network formers. For instance, a glass formed by melting one mole of CaO,

one mole of $K_2O$, and five moles of $SiO_2$ together is written in the mole formula presentation as $K_2O{\cdot}CaO{\cdot}5SiO_2$.

To convert this to a mole fraction basis, note that there are seven molecules in all, and hence the formula will be $0.143K_2O{\cdot}0.143CaO{\cdot}0.715SiO_2$ (neglecting the rounding-off error). The conversion to mol % is obtained simply by multiplying this formula by 100, i.e., the formula will be $14.3K_2O{\cdot}14.3CaO{\cdot}71.5SiO_2$ (mol %).

To convert this to a weight percent (abbreviated wt. %) basis, one notes the atomic weights: K = 39, O = 16, Ca = 40, and Si = 28. Thus, one formula weight of $K_2O{\cdot}CaO{\cdot}5SiO_2$ has 94 grams $K_2O$, 56 grams CaO, and 300 grams $SiO_2$, totaling 450 grams. This yields $20.9K_2O{\cdot}12.4\ CaO{\cdot}66.7SiO_2$ (wt. %). The reverse process, i.e., conversion from wt. % to mol %, should be obvious.

The reader may readily show that a soda lime glass composition does not change much in converting from mol % to wt. %.

Sometimes, glasses have minor constituents, added deliberately or by way of contamination. Colorants and glass fining agents are good examples of the deliberate additions. On the other hand, except for the production of amber glass, Fe is invariably a contaminant (coming primarily from the tools used for the mining of the raw materials). The minor constituents are often listed at the end of the glass formula, presented as oxides (e.g., FeO, $As_2O_3$), elements (e.g., Co, F), and groups (e.g., $SO_4^{2-}$). Where an ion may be present in the multivalent form (e.g., $Fe^{2+}$ and $Fe^{3+}$), and the exact ratio of the two is not known, it is conventional to lump the two into one form. (The student may therefore show that the glass composition may occasionally not add up to 100% despite all the accuracy of a chemical analysis.)

Unfortunately, the convention of presenting the oxide glasses is not maintained for the case of other glass systems. In fluoride glasses, the network former is listed first, with no particular order to the rest. In chalcogenides, the listing is done in order of the chemical group number. Fortunately, this leads to the glass chain former being listed last. In metallic glasses, the listing is done in increasing order of content.

The reader may also recognize that the wt. % formulation is convenient for glass-melting, etc., whereas the mole formula and the mol % presentations give better intuitive feeling for the glass structure and properties.

## 5.2. Silica Glass

Suggested reading: A. C. Wright, A. G. Clare, D. I. Grimley, and R. N. Sinclair, *J. Non-cryst. Sol.* **112**, 33–47 (1989).



The structure of silica glass is the simplest of all the glass structures, yet many of the details are not yet fully understood.

As shown in Fig. 3-1, glass consists of slightly distorted $SiO_4$ tetrahedra joined to each other at corners. The basic unit is shown in Fig. 5-1a. Each oxygen acts as a bridge between neighboring tetrahedra (Fig. 5-1b), and hence is called a **bridging oxygen**, or simply a **BO**. Nearly 100% of the oxygens are bridging except for some defect sites and for those associated with impurities in commercial specimens. Angle $\beta$ between two neighboring tetrahedra ($=Si_1{-}O_4{-}Si_2$ angle) is called the **bond angle**. Torsion angles $\alpha_1$ and $\alpha_2$ are, respectively, the azimuth angle between $Si_1{-}O_1$ and $O_4{-}Si_2$ when projected on the $O_1{-}O_2{-}O_3$ plane, and the rotation angle about the $O_4{-}Si_2$ axis. (The subscripts are used to identify the various atoms in Fig. 5.1b.) The glass is then made up of the $SiO_4$ tetrahedra joined to each other at the bridging oxygen corners (Fig. 5-1c). *The disorder of the glass structure is ascribed mostly to the variations in the bond angle $\beta$ and the torsion angles $\alpha_1$ and $\alpha_2$, and to some extent to the variation in bond lengths.*

Figure 5-1a describes the short-range (range I) structure extending out to about 2.5 Å. It includes the types of the various atoms, their local coordination sphere, and the two nearest-neighbor distances, $Si_1{-}O_1$ and $O_1{-}O_2$. The range II structure ($\sim$2.5–5 Å) is described by the bond angle and the torsion angles (and hence, the distances to the atoms in a neighboring tetrahedron) (Fig. 5-1b). The intermediate range (range III) primarily constitutes the shortest-path ring size in Fig. 5-1c (ring statistics) and topological information. The long-range structure (beyond $\sim$10–20 Å), depicted as complete Fig. 5-1c, describes density and phase composition fluctuations.

The pair distribution function, curve A, extracted from XRD data by Mozzi and Warren (1), is shown in Fig. 5-2a. The peaks become broader as the distance between a pair of atoms increases because of the effect of randomness. The locations of the peaks give the various ion pair distances, which are listed in Table 5-1. The first peak corresponds to the Si–O first coordination shell. The area under the peak yields an oxygen coordination of $\sim$4.0 about each silicon, indicating that the Si–O polyhedra are rarely anything but tetrahedra. The average tetrahedral angle $O_1{-}Si_1{-}O_2$ is $\sim 109°$. One may, however, note that the $O_1{-}O_2$ peak describing the short-range structure in Fig. 5-2a is already not too well defined. As a result, after achieving an empirical fit (curve B) to the short-range structure, a large unexplained residual (curve C) corresponding to the intermediate-range structure remains in Fig. 5-2a. Thus, the accuracy of the medium- and long-range structural information extracted from the XRD data could be questioned. Fortunately, the $O_1{-}O_n$ ($n = 2, 3, 4$) component correlation can be resolved quite well using neutron diffraction (Fig. 5-2b). The nearest-neighbor distance is the $Si_1{-}O_1$ bond at 1.62 Å. The tetrahedral edge $O_1{-}O_2$

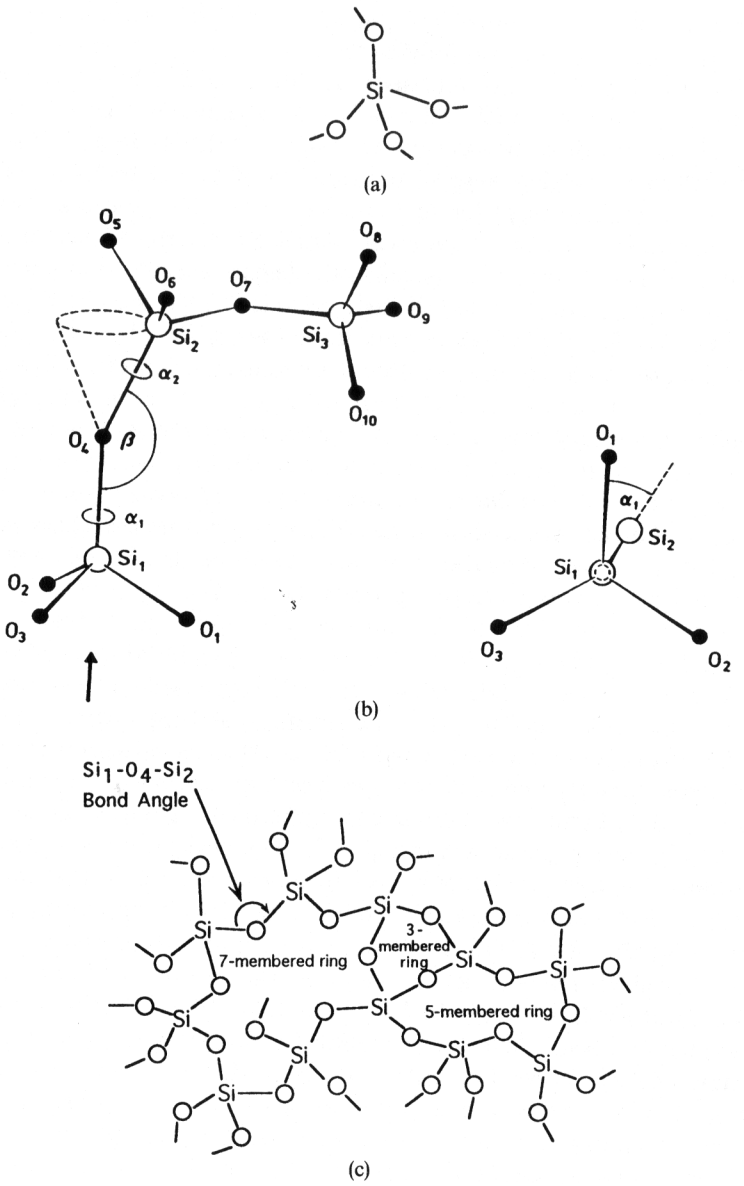


**Figure 5-1.** (a) Basic building block for silica glass. $SiO_4$ tetrahedron with all four oxygens bridging between neighboring tetrahedra. (b) Definition of the bond angle $\beta$ and the torsion angles $\alpha_1$ and $\alpha_2$. (After A. C. Wright, G. A. N. Connell, and J. W. Allen, *J. Non-cryst. Sol.* **42**, 69 (1980). Reproduced with permission of Elsevier Science Publishers.) (c) Schematics of the silica glass network, defining the "bond angle" and the ring structures.



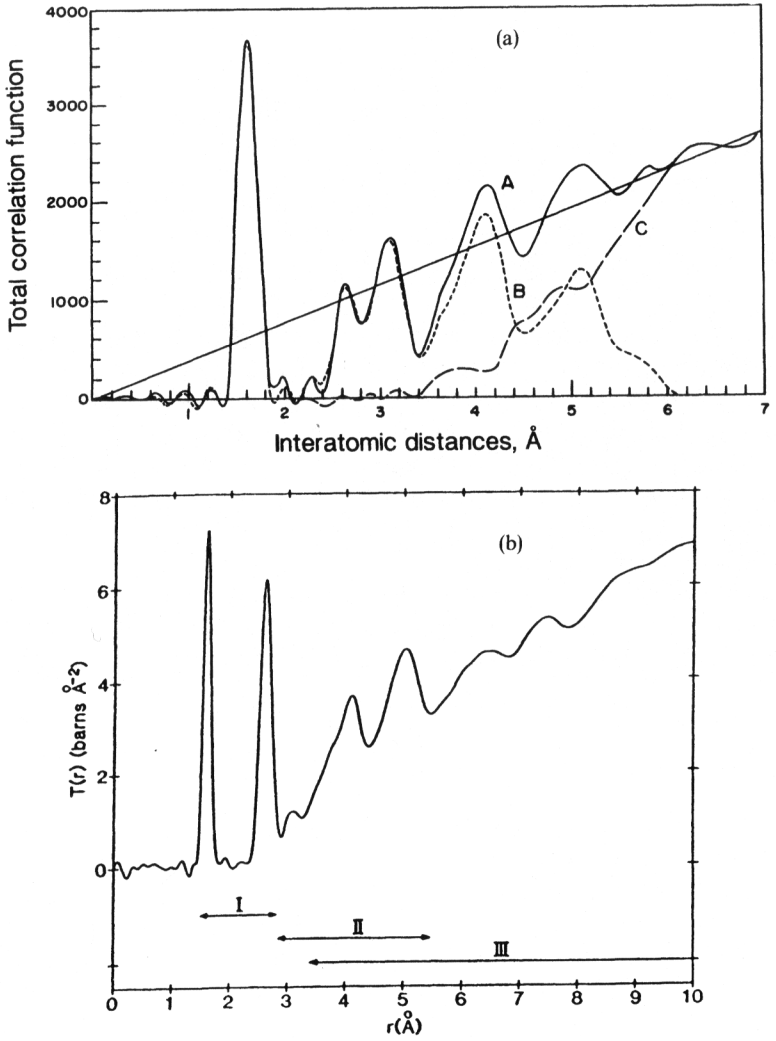


**Figure 5-2.** (a) The total correlation function for fused silica, measured by Mozzi and Warren (1) using x-ray. A is the measured curve; B is the sum of the calculated curve for the six contributions: $Si_1$–$O_1$, $O_1$–$O_2$, $Si_1$–$Si_2$, $Si_1$–$O_6$, $O_1$–$O_6$, and $Si_1$–$Si_3$. Curve C is the difference between A and B. (Reproduced with permission of Munksgaard International Publishers Ltd., Copenhagen.) (b) The total correlation function of fused silica measured using neutron diffraction. The roman numerals define the various ranges of structures. Note a better definition of the $O_1$–$O_2$, and not so good a definition of the $Si_1$–$Si_2$ peak. (After A. C. Wright, R. A. Hulme, D. I. Grimley, R. N. Sinclair, S. W. Martin, D. L. Price, and F. L. Galeener, *J. Non-cryst. Sol.* **129**, 213 (1991). Reproduced with permission of Elsevier Science Publishers.

**Table 5-1.** Ionic Pair Distances in Vitreous Silica

| | |
|---|---|
| $Si_1$–$O_1$ | 1.62 Å |
| $O_1$–$O_2$ | 2.65 Å |
| $Si_1$–$Si_2$ | 3.12 Å |
| $Si_1$–$O_6$ | 4.15 Å |
| $O_1$–$O_6$ | ~5.0 Å |
| $Si_1$–$Si_3$ | ~5.0 Å |

is about 2.65 Å. The peak at about 5.8–6 Å in Fig. 5-2b is, perhaps, due mostly to silicon–third oxygen (e.g., $Si_1$–$O_8$) distance. Beyond about 6 Å, the pair distribution function tends to approach the random probability and it becomes hard to assign the various peaks. *The bond angle distribution from the XRD data ranges between* 120° and 180° (Fig. 5-3) *with a maximum at* ~144°. The number of atoms within a ring may vary considerably—generally from 5 to 10 or more. The ring statistics, however, are quite sensitive to the structural model employed.

**Modeling of silica glass structures** has been attempted by Bell and Dean [2] using polystyrene spheres to represent silicon and oxygen atoms and 1/16 inch steel wires to represent the bonds between them (Fig. 5-4). Evans and

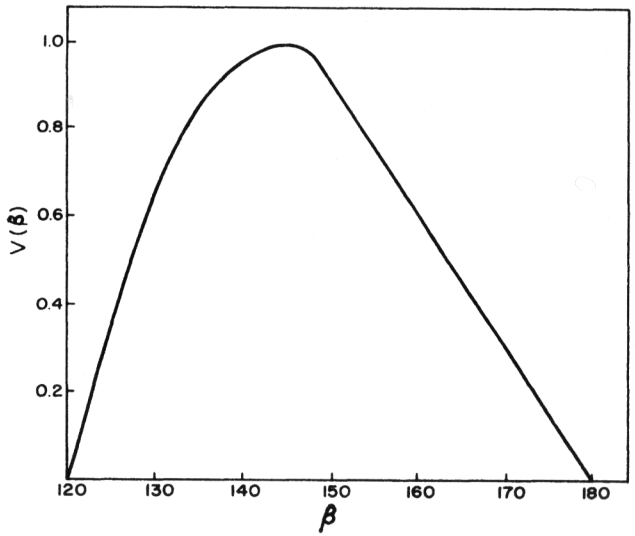


**Figure 5-3.** The distribution of the Si–O–Si bond angles in fused silica (after Mozzi and Warren [1]. The ordinate $V(\beta)$ is the fraction of bonds with bond angles $\beta$ normalized to the most probable angle. (Reproduced with permission of Munksgaard International Publishers Ltd., Copenhagen.)



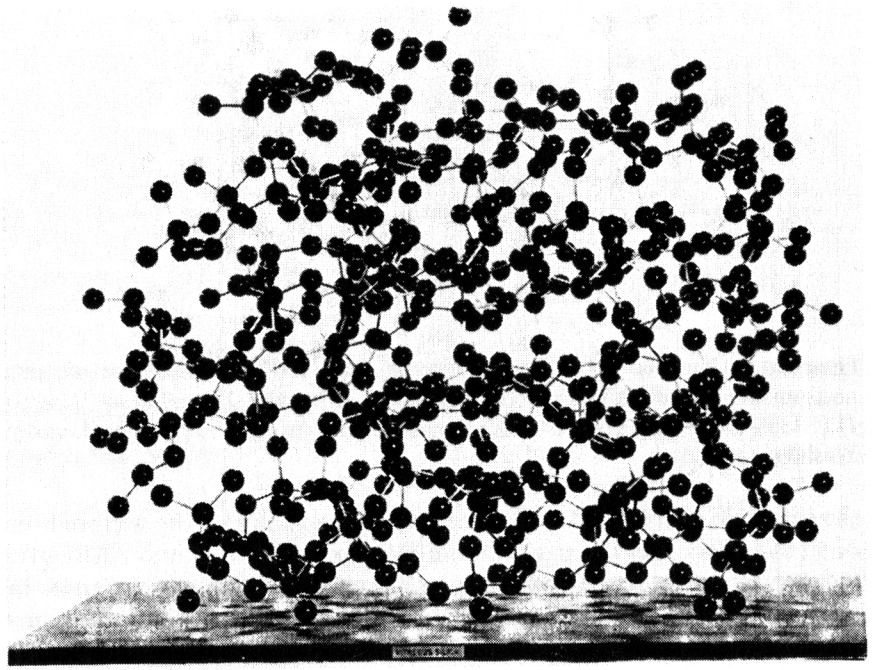

**Figure 5-4.** Continuous random network model of vitreous silica structure. (After R. J. Bell and P. Dean, *Nature* (London), **212**, 1354 (1966).

King [3] used tetrapods and springs to construct the tetrahedra. The basic rules for the construction of the models were adopted from Zachariasen's random network theory. After the construction, the distances between the various ions were measured to give the radial distribution function for various ion pairs in the model. Fig. 5-5 shows the excellent agreement obtained by Bell and Dean between the silica RDF obtained by XRD and that computed for the model.

Computer simulations of silica glass structure have also been attempted using the method of **molecular dynamics** (MD) by Soules [4], the **Monte Carlo technique** by Wooten and Weaire [5], and **normal coordinate analysis** by Cherukuri [6]. In the method of molecular dynamics, one starts with a certain number of constituent ions with given mass numbers that occupy random positions in a defined box such that the density at room temperature matches the experimentally observed value. The potentials at each ion are then described. These may be two-body, three-body, or multibody potentials. The derivative of the potential with respect to the interionic distance gives an interionic force. Forces also arise randomly because of the kinetic energy of

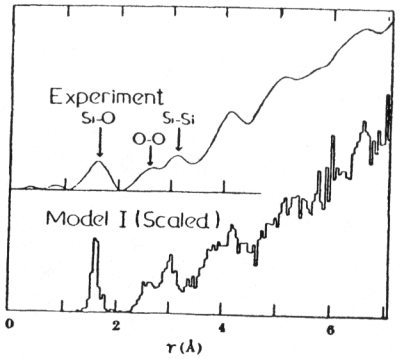


**Figure 5-5.** Comparison of the experimental x-ray RDF for fused silica and that measured for the Bell and Dean model. (After R. J. Bell and P. Dean, *Nature (London)* **212**, 1354 (1966). Reproduced with permission of Nature Publishing Company, Washington D.C.)

the ensemble (determined by the prescribed temperature). The vectorial sum of all the forces, and the application of Newton's laws of motion, then gives for each ion a vectorized acceleration that, upon integrating twice, gives the change in position of each ion over a given time step. The box is first thermalized for a predetermined time at a very high temperature (generally as much as 5,000 °C). The temperature is lowered, and thermalization again carried out. In this way the box is brought essentially to room temperature. Finally, all the relevant information regarding structural details, such as pair distribution function, bond angles, force constants, vibrational frequencies, etc., and dynamic parameters such as the diffusion coefficient of the various ions, are computed. To make representative calculations using MD techniques, one often needs as many as 1,000 ions and 5–10,000 time steps of $10^{-15}$ seconds each. In order to make the relatively small box containing 1,000 atoms more representative of a much larger volume of material, the device of 'periodic boundary conditions' on the walls is imposed. Thus, if calculations predict an atom leaving one face of the box with a particular velocity, the program automatically introduces an identical atom entering the opposite face with the same velocity. The small value of the time step (very much less than a jump frequency interval) is necessary to avoid errors in numerical integration. It is clear then that even with the fastest computers it is difficult to allow any more than a few picoseconds for the glass to cool down from a high temperature to room temperature—which does not represent reality. One further difficulty involved with MD calculations is the simulation of other than ionic potentials that are spherically symmetric. (Recent advances in this direction include the use of Stillinger and Weber three-body potentials [7].) In spite of the inability to exactly



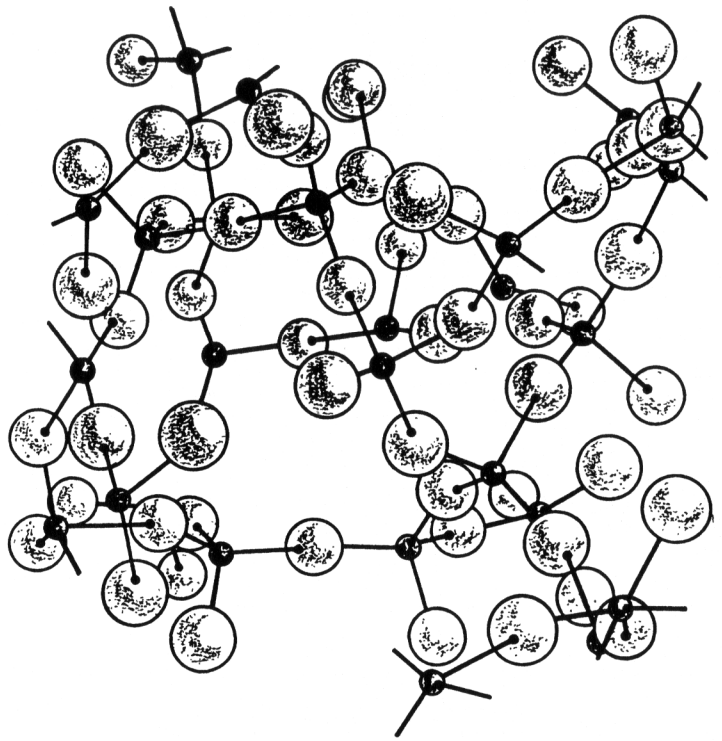

(a)

**Figure 5-6.** (a) Molecular dynamic simulation of the vitreous silica structure. (After T. F. Soules, *Glass Sci. & Tech.* **4A**, Fig. 31, p. 318 (M. Tomozawa and R. H. Doremus, eds.). Academic Press, New York, 1990.)

simulate the interionic potentials and the limitations to computer power currently available, the molecular dynamics method has proven remarkably effective in simulating glass structures and in gaining some insight into factors that influence glass properties. Fig. 5-6a shows a computer simulation of the silica glass structure. The individual pair distribution functions are shown in Fig. 5-6b. Note that the ionic distances match those in the experimentally measured RDF. Detailed analysis shows that the ion coordinations are also duplicated quite well. However, the mismatch observed in the sharpness of the peaks suggests that the variations in bond length and bond angles may not be correct. This would clearly affect the agreement over the medium-range order; in particular, the ring statistics may not be predicted accurately.

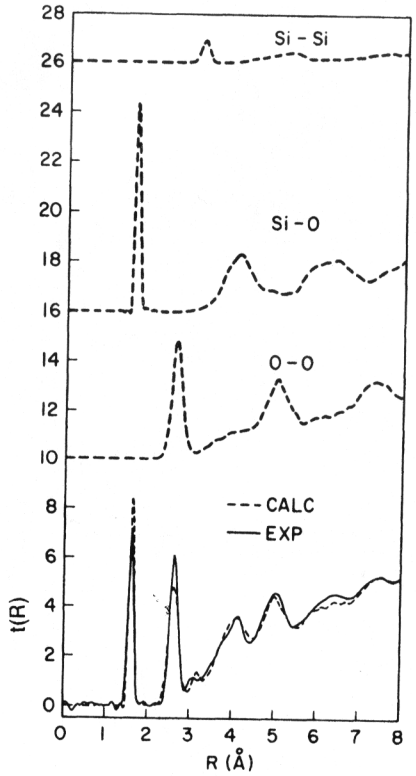


(b)

**Figure 5-6.** (b) Individual pair correlation functions, $t(r)$, for Si–O, Si–Si, and O–O obtained from MD calculations. A calculated composite RDF is compared with that measured using neutron diffraction. (After T. F. Soules, *Glass Sci. & Tech.* **4A**, Fig. 33, p. 320 (M. Tomozawa and R. H. Doremus, eds.). Academic Press, New York, 1990.)

Because of the high degree of connectivity, the values of mass transport properties, e.g., fluidity, in silica glass are very low (i.e., the viscosity is high).

## 5.3. Boric Oxide Glass

In $B_2O_3$ glass, the oxygen coordination around each B is only 3, and hence the basic structural unit is a $BO_3$ triangle. It is believed that B is slightly above the plane of the three oxygens. Again, all the oxygens are bridging between neighboring triangles. Several authors believe that the basic building



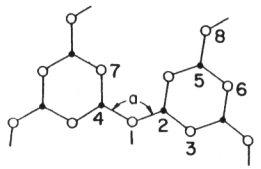

**Figure 5-7.** Configuration of the boroxol ring.

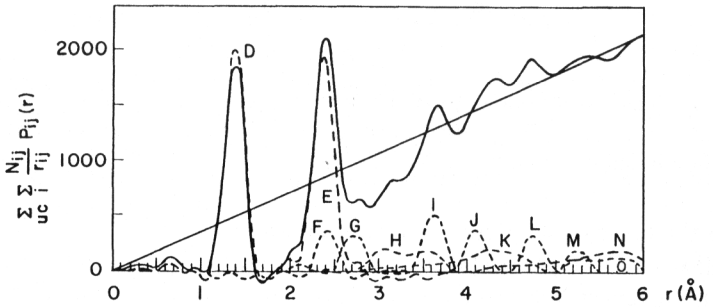


**Figure 5-8.** Total correlation function of vitreous $B_2O_3$. Dashed curves correspond to various ion pairs shown in Fig. 5-7 with distances (Table 5-2) suggested by Mozzi and Warren [8]. Note that MD calculations reveal the B–B peak to be at 0.273 nm (where peak G is located). (Reproduced with permission of Munksgaard International Publishers Ltd. Copenhagen.)

**Table 5-2.** Ion Pair Distances in Vitreous $B_2O_3$

| Peak | Kind of atoms | Designation on figure | Interatomic distance | $\sum_{uc}\sum_{i} N_{ij}$ |
|---|---|---|---|---|
| D | B–O | 1-2 | 0.137 nm | 12 |
| E | O–O | 1-3 | 0.237 | 12 |
| F | B–B | 2-4, 2-5 | 0.243 | 6 |
| G | B–O | 2-6 | 0.274 | 4 |
| H | B–O | 2-7 | variable | 8 |
| I | B–O | 2-8 | 0.363 | 8 |
| J | O–O | 3-8 | 0.410 | 4 |
| K | O–O | 3-7 | variable | 8 |
| L | O–O | 1-8 | 0.475 | 4 |
| M | B–O | 4-6 | 0.525 | 4 |
| N | B–O | 5-7 | variable | 16 |
| O | B–O | 4-8 | variable | 8 |

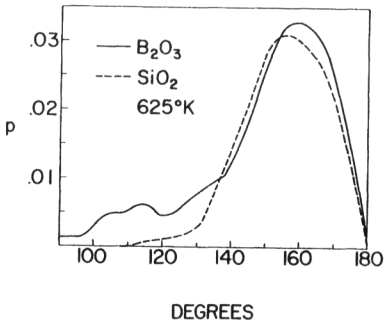


**Figure 5-9.** The distribution of the B–O–B bond angles in vitreous $B_2O_3$ compared to the Si–O–Si bond angles in fused silica (using MD calculations). The ordinate is the absolute fraction of bonds per degree angle.

block in the boric oxide glass is the **boroxol group** shown in Fig. 5-7. A pair distribution function plot [8] from XRD is shown in Fig. 5-8, and the various interionic distances are tabulated in Table 5-2. Note that the G peak at 0.274 nm (=2.74 Å) distance was assigned to the B-cis O in the boroxol group, and the B–B peak (F peak) corresponding to a distance of 0.243 nm was assumed to be concealed under the E peak. Molecular dynamic calculations (9), on the other hand, show that the B–B distance is 0.272 nm (and

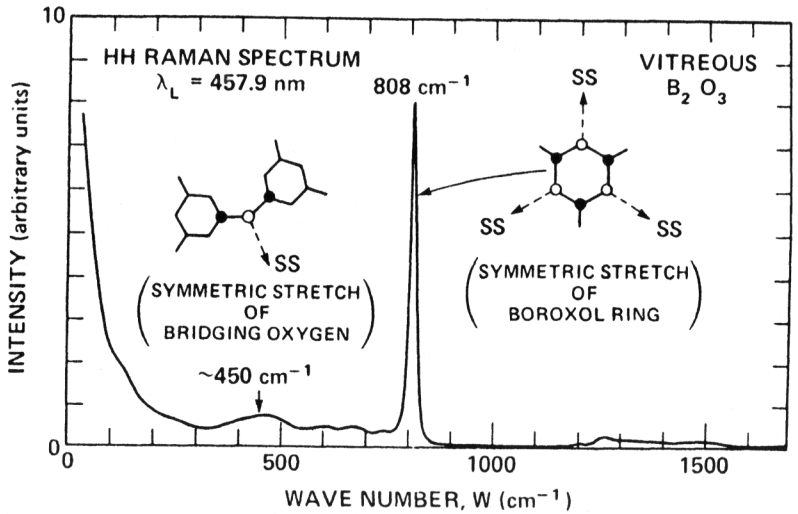


**Figure 5-10.** Assignment of the two highly polarized modes in the Raman spectrum of vitreous $B_2O_3$. (After F. L. Galeener, in *The Structure of Non-crystalline Materials 1982* (P. H. Gaskell, J. M. Parker, and E. A. Davis, eds.), Fig. 5, p. 343. Taylor & Francis, Inc., New York, 1983.) Reproduced with permission of the publisher.)



not 0.243 nm), and hence is the G peak. The absence of a significantly large population of 120° angles in the B–O–B bond angle distribution (Fig. 5-9) also suggests the presence of only a low number of the boroxol groups.

Perhaps the strongest support to the concept of boroxol rings has been derived from the Raman spectrum of $B_2O_3$ glass shown in Fig. 5-10. The peak at 808 $cm^{-1}$ is ascribed to the symmetrical stretching of the boroxol ring.

Some research has shown that the equilibrium (boroxol) $\Leftrightarrow BO_{3/2}$ triangle shifts to the right with increasing temperature. This would explain why the high-temperature structures obtained by MD techniques do not show much concentration of the boroxol groups. Whatever the nature of the ring configurations is, the triangular connections in the $B_2O_3$ glass do not make a very rigid structure. Hence, many transport properties of $B_2O_3$ glass have high values typical of fluid structures.

## 5.4. Alkali Silicate Glasses

The range of glass formation in the various alkali silicates determined by means of conventional melting techniques is continuous from $SiO_2$ up to about 36 mol % $Li_2O$, about 58 mol % $Na_2O$, and about 55 mol % $K_2O/Rb_2O/Cs_2O$.

As indicated in Section 3.1.2, *the alkalis are network modifiers; they enter the glass as singly charged cations and occupy interstitial sites.* The unit positive charge is satisfied by an ionic bond to an oxygen. This is accomplished by breaking a bridge and attaching an oxygen (provided by the alkali oxide $M_2O$) to the broken bridge, as shown by the reaction

$$\begin{array}{c} | \\ -Si-O-Si- \\ | \quad | \end{array} + M_2O = \begin{array}{c} | \\ -Si-O^-M^+ \\ | \end{array} \quad \begin{array}{c} | \\ M^+{}^-O-Si- \\ | \end{array} \qquad (5.1)$$

Thus, *each alkali ion is expected to create one "nonbridging oxygen (NBO)."* A schematic representation of an alkali silicate network is shown in Fig. 5-11. *The creation of NBO in the network reduces the connectivity*, and hence, mass-transport-related properties such as fluidity (inverse of viscosity), diffusion, electrical conduction, and chemical corrosion increase. For similar reasons, the structure acquires the freedom to expand, for instance, its thermal expansion coefficient increases.

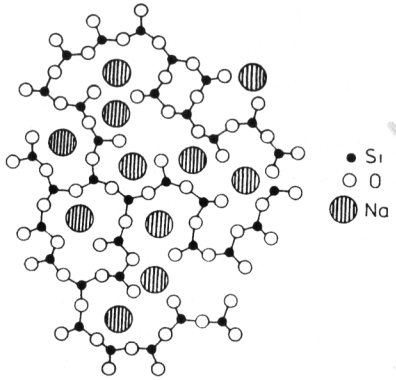


**Figure 5-11.** Two-dimensional representation of the structure of sodium silicate glass. (The fourth oxygen with every Si is presumed to be out of the plane of the paper.) Note that some oxygens (bridging oxygens) are coordinated to two silicons, others to only one. In the latter case (nonbridging oxygen), a sodium ion will be found in the vicinity for charge compensation.

To determine the fraction of NBO, one first converts the glass formula to a mole basis, and proceeds as follows:

*Example*: For $20Na_2O{\cdot}80SiO_2$ (mol %) glass

Since $\#\ Na^+ = 40$, hence $\#$ NBO $= 40$.
Since total oxygens $= 180$, $\#$ tetrahedra ($\square$) $= \#$ silicon atoms $= 80$,
hence $f_{NBO}$ = fraction of NBO of the total oxygens $= 40/180 = 0.22$
$f_{BO} = 140/180 = 0.78$, and $\#$ BO/$\square = 140/80 = 1.75$

$Y = \#$ of corners shared/$\square = 2 \times \#$ BO/$\square = 3.5$ (because each BO is shared by two $\square$)

$Y$ can also be calculated using the formula

$$Y = 6 - 200/p, \quad \text{where } p = \text{mol \% } SiO_2 \tag{5.2}$$

Using Eq. (5.2), it can be readily seen that $Y = 2$ at 50 mol % $SiO_2$. The tetrahedra then form linear chains or isolated rings—there is a clear breakdown of the 3-D network at 50 mol % $SiO_2$. At 40% $SiO_2$, $Y = 1$. This implies that only one corner/$\square$ is shared. The structure of an alkali silicate then contains isolated pairs of tetrahedra (or a mixture of isolated single tetrahedra and longer chains), as shown in Fig. 5-12. Apparently, as stated earlier, glass formation continues to occur even in these less than 3-D connected structures. It has been suggested that bonding in glasses with



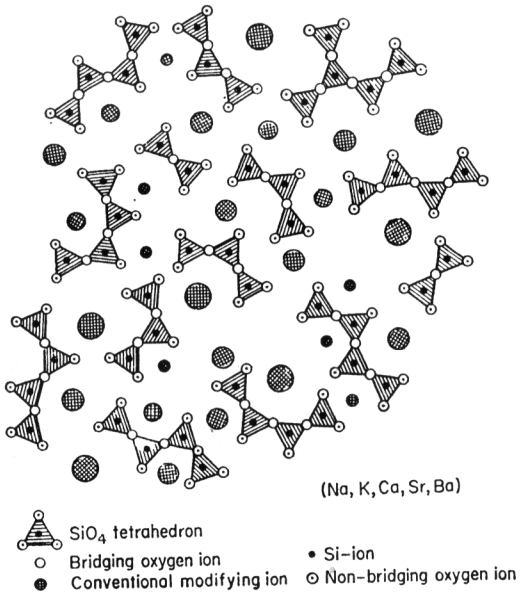


**Figure 5-12.** Two-dimensional representation of an "invert glass."

$Y = 2$ or less is accomplished by the van der Waals forces between the alkali ions, thus "inverting" their role; hence the name **invert glass** for this class of glasses. A plot of log $\eta$ versus $Y$, where $\eta$ is the viscosity, is shown in Fig. 5-13 and suggests the increase in the tightness of bonding with alkali increasing below $Y = 2$.

In recent years, one other powerful tool developed to elucidate the environment of the various nuclei in glass is the **magic-angle spinning nuclear magnetic resonance** [10] **(MAS-NMR)** technique. In an NMR experiment, a nucleus possessing a magnetic moment is spun at an angle $\theta$ to an externally applied magnetic field $H_0$, causing the nucleus to precess at Larmor frequency about the field axis. An oscillating electromagnetic field of the same frequency is then allowed to interact. The resulting nuclear resonance then causes absorption of energy from the oscillating field proportional to the Boltzmann distribution of the nuclear spin populations and the effective nuclear relaxation times. The NMR spectra are affected by the chemical-shift anisotropy interaction resulting from the shielding of $H_0$ by the electrons surrounding the resonating nucleus. Any change in the local electron density around the nucleus, such as those resulting from a coordinate change, can be detected. It is found that the Hamiltonians describing the dipolar, chemical shift, and first-order quadrupolar interactions are all multiplied by a factor $\beta = (3\cos^2\theta - 1)$. When $\theta = 54.74°$, $\beta = 0$, which removes, in effect,

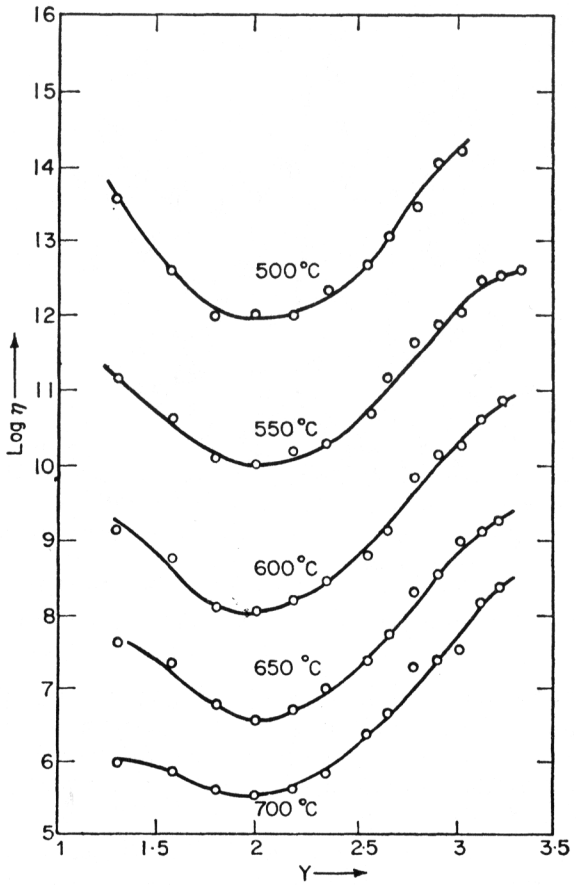


**Figure 5-13.** Viscosity isotherms of $Na_2O$–$K_2O$–CaO–SrO–BaO–silicate glass as a function of the structural parameter $Y$ ( = average number of corners shared per tetrahedron).

all the peak broadening interactions in the NMR spectra. (That is why $\theta = 54.74°$ is called the 'magic angle'.)

In alkali silicate glasses, the chemical-shift anisotropy on $^{29}Si$ yields information regarding the second neighbors, particularly the identification of bridging and nonbridging oxygens. The local configuration around the $^{29}Si$ atom is expressed as $Q_n$ (n = 0 to 4) units, where $Q_0$ represents all NBO's (isolated $SiO_4$ tetrahedron), and $Q_4$ represents all BOs. At any value of $x$ ($0 < x < 1$) in $(M_2O)_x(SiO_2)_{1-x}$ glasses, statistical arguments for a random model would predict the presence of all $Q_n$ the relative numbers of which are determined by $x$. The ordered model, on the other hand, predicts



for certain stoichiometric compositions only specific $Q_n$ units, for instance, $Q_3$ at $x = 0.33$, and $Q_2$ at $x = 0.5$ (see example above). The results of MAS-NMR for $0.33 < x < 0.5$ support the ordered model: at $x = 0.33$, only $Q_3$ are present which transform completely to $Q_2$ at $x = 0.5$. In the intermediate range of compositions, both $Q_3$ and $Q_2$ are present. The amount of $Q_4$ present, if any, is much less than that expected from the random model. Some recent results of Maekawa *et al.* [10b] for the Li, Na, and K silicates suggest an equilibrium reaction:

$$2Q_n \Leftrightarrow Q_{n-1} + Q_{n+1} \ (n = 3, 2, 1 \text{ for Na and K, and } n = 3, 2 \text{ for Li}).$$

A plot of $\%Q_n$ against mol % alkali for the three systems is shown in Fig. 5-14.

In summary, it may be confidently said that the addition of one alkali ion creates one NBO. However, *the occurrence of the NBOs in the network is not entirely random.* Measurements of ionic diffusivity and electrical conductivity strongly suggest that alkalis, and hence the NBOs, occur in pairs. (This is the basis of writing the reaction [5.1] shown earlier.) Calculations of

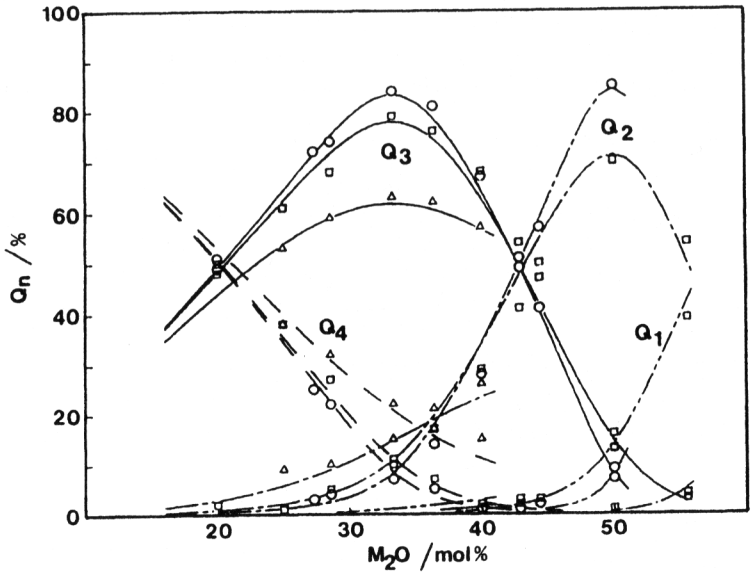


**Figure 5-14.** Experimentally determined $Q_n$ distribution using MAS-NMR in lithium (△), sodium (□), and potassium (○) silicate glasses as a function of mol % alkali oxide. Curves represent theoretical fitting. (After H. Maekawa, T. Maekawa, K. Kawamura, and T. Yokokawa, *J. Non-cryst. Sol.* **127**, 53–64 (1991). Reproduced with permission of Elsevier Science Publishers.)

the pair distribution function using the method of MD, performed by Soules, also suggest larger than random probability for the occurrence of paired alkalis.

## 5.5. Alkali–Alkaline Earth–Silicate Glasses

The range of glass formation in alkali–alkaline earth–silicate glasses is shown on the ternary composition space in Fig. 5-15. In general, the various alkalis and alkaline earths can be introduced to a little over 50 mol % total.

The alkaline earth cations are bivalent, and like the alkalis, *they occupy interstitial spaces as glass network modifiers.* The addition of one alkaline earth creates two nonbridging oxygens. The connectivity in the process is still maintained to a large extent, and hence alkaline earth additions to alkali silicates greatly stabilize the glass network. (For instance, the glass no longer readily dissolves in water!) The phase equilibrium diagram in the soda-lime system is shown in Fig. 5-16 (%$Na_2O$ is calculated by difference from 100). The lowest liquidus temperature (725°C) occurs at the ternary eutectic joining the quartz, devitrite ($Na_2O{\cdot}3CaO{\cdot}6SiO_2$), and sodium disilicate ($Na_2O{\cdot}2SiO_2$) phase fields. Superimposed upon the figure are the lines of equal crystal growth rate [11] (the numbers are seconds for a 10-micron

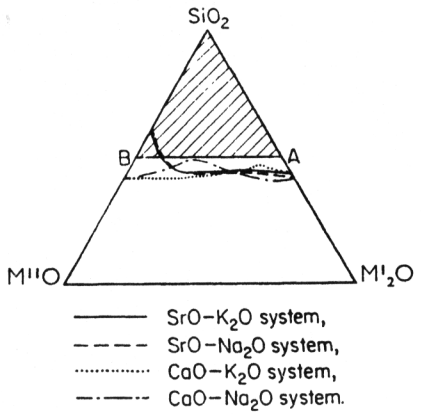


**Figure 5-15.** Glass-formation regions in various ternary silicate glasses. M′ is a monovalent atom, and M″ is a divalent atom. (After M. Imaoka, *Adv. in Glass Tech.*, Part I, p. 149. Plenum Press, New York, 1962. Reproduced with permission of the publisher.)



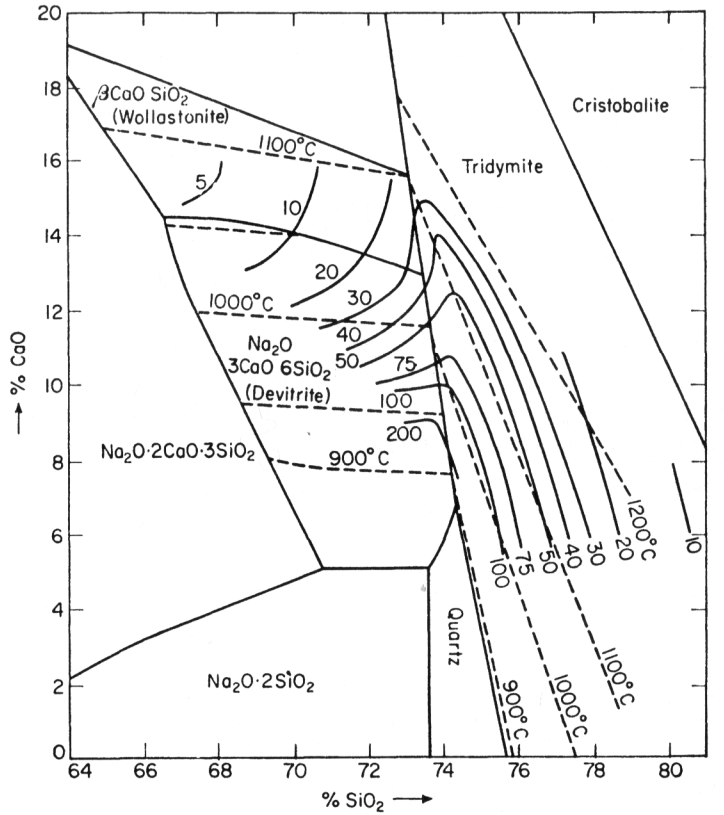


**Figure 5-16.** Phase diagram in the $Na_2O$–CaO–$SiO_2$ system ($Na_2O$ is given by the difference from 100 wt. %). Lines of equal crystal growth rate (seconds for a 10 micron growth) are superimposed. (After H. Rawson, *Inorganic Glass-Forming Systems*, Fig. 35, p. 88. Academic Press, London, 1967.)

crystal to grow). The glass-forming region of commercial interest is about half of the devitrite phase field near the ternary eutectic. The calculations of $f$ and $Y$ in the alkali–alkaline earth–silicate glasses can be made in the same manner as for the alkali silicates.

## 5.6. Alkali Borate Glasses

The boron ion is trivalent positive and is a glass former. The introduction of an oxygen from a modifier oxide to boric oxide glass brings about one of the two possibilities:

(a) *Create a nonbridging oxygen*, as in the silicate glasses, by forming $BO_{2/2}O^-M^+$. (The "/2" subscript is used to identify the connection to two cations.)

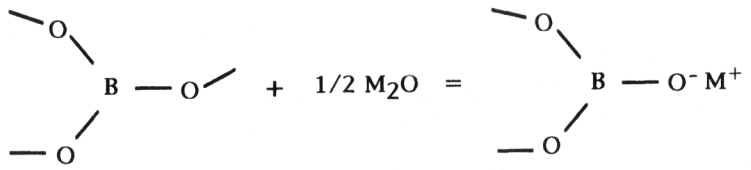


The oxygen coordination around the boron remains three.

(b) *Convert boron from a 3-coordination state* ("$B_3$ *state*") *to a* 4*-coordination state* ("$B_4$ *state*"). Boron in a tetrahedrally coordinated state is known to exist in some crystalline borates.

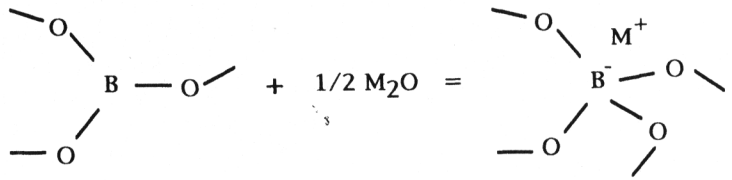


In the $BO_3$ group, the oxygens are fully bridging, and hence one negative charge from each oxygen satisfies the three positive charges on the boron ion. After the conversion from $B_3$ to $B_4$, all the oxygens remain bridging; the extra negative charge on the $[BO_{4/2}]^-$ group is satisfied by an alkali $M^+$ ion in the vicinity. The electron transfer from the M atom occurs as a distributed charge density over a large-effective-diameter $BO_4$ group, and not localized between the M atom and any specific oxygen. Since this association is somewhat loose, the alkali ion is expected to become more mobile. At the same time, the connectivity of the network increases, and hence flow-related properties decrease (i.e., viscosity increases) and thermal expansion decreases.

It is possible that, like the boroxol $\Leftrightarrow 3BO_{3/2}$ equilibrium, the $[BO_{4/2}]^-M^+ \Leftrightarrow BO_{2/2}O^-M^+$ equilibrium also shifts to the right as the temperature increases.

## 5.7. The Boron Anomaly

Gooding and Turner's data [12] on the thermal expansion coefficient of sodium borate glasses as a function of the added alkali is shown in Fig. 5-17a. Note that the expansion coefficient shows a marked minimum at about



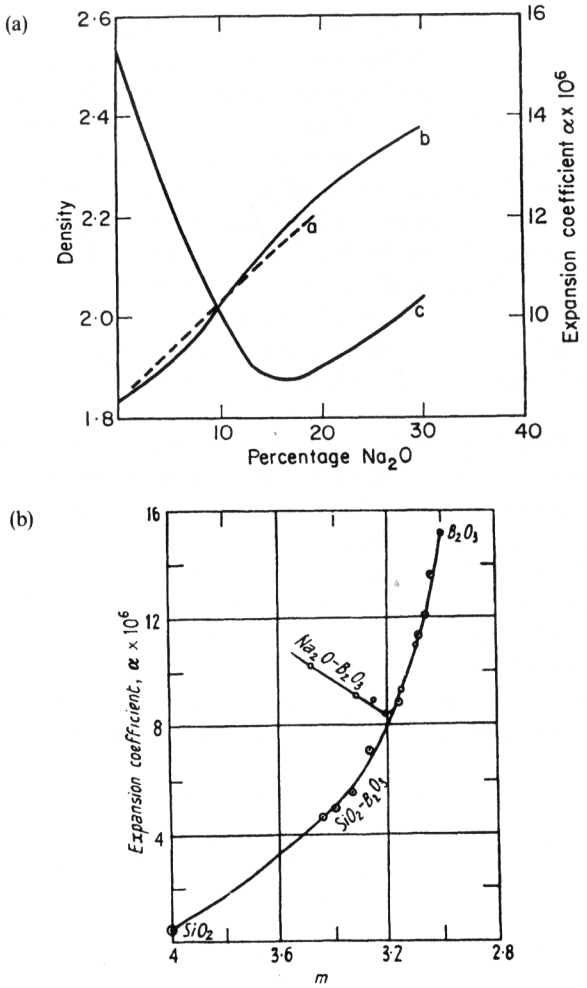


**Figure 5-17.** (a) Thermal expansion coefficient and density of $Na_2O$–$B_2O_3$ glasses: curve "a," calculated density; curve "b," measured density; curve "c," measured thermal expansion coefficient. (b) Thermal expansion coefficients plotted against average coordination number $m$ for the systems $SiO_2$–$B_2O_3$ and $Na_2O$–$B_2O_3$.

16 wt. % $Na_2O$. (More recent data also show that, in addition to the minimum in the expansion coefficient, the glass transformation temperature $T_g$ at which viscosity = $10^{12}$ Pa·s shows a maximum.) This extremum behavior (instead of the almost linear change with composition found in silicate glasses) was termed "**the boron anomaly**." Biscoe and Warren [13] explained the anomaly by suggesting that, initially, *the addition of each alkali ion to*

*boron oxide causes one boron to change from the $B_3$ state to the $B_4$ state. No NBOs are created.* The increased connectivity, hence, causes the thermal expansion to decrease and viscosity to increase. The conversion stops at around 16 mol % added alkali. Thereafter, further additions cause the production of NBOs, and a resultant increase in expansion and decrease in viscosity. To support this hypothesis, Warren [14] plotted the expansion coefficient of borosilicate glasses and sodium borates together against an average coordination number, $m$, for the network-forming cations in the glass (see Fig. 5-17b). The borosilicate data plot as a smooth curve between $m = 4$ for $SiO_2$ at one end and $m = 3$ for $B_2O_3$ at the other end. The $m$ value for the sodium borates was calculated using the preceding premise that one added alkali raises one boron from the $B_3$ state to the $B_4$ state. The sodium borates superimpose well on the curve from $m = 3$ to about $m = 3.17$. At higher values of $m$, the data depart sharply upwards. The value $m = 3.17$ corresponds to about 13 wt. % $Na_2O$. Warren's notion of 3 to 4 coordination change for boron and its subsequent termination as the explanation of the origin of boron anomaly met wide acceptance.

Later, Bray and O'Keefe [15] experimentally determined the fraction, $N_4$, of the 4-coordinated boron ($= \#B_4/\#$total borons) in the alkali borates using NMR. Their results are shown in Fig. 5-18. For $xM_2O{\cdot}(1-x)B_2O_3$ glass, the total number of borons are $2(1-x)$, and if every $M^+$ converts one boron from $B_3$ to $B_4$, then $\#B_4 = \#M = 2x$. This should yield $N_4 = x/(1-x)$. The solid curve on the figure corresponds to $N_4 = x/(1-x)$.

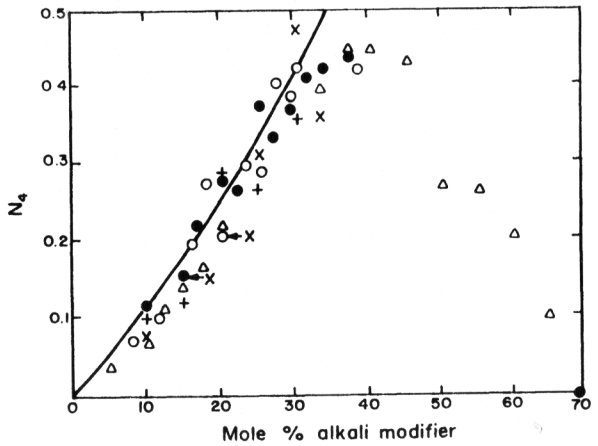


**Figure 5-18.** The fraction $N_4$ of 4-coordinated boron atoms in alkali borate glasses as a function of mol % alkali. $Na_2O$ (•); $K_2O$ (○); $Li_2O$ (△); $Rb_2O$ (+); $Cs_2O$ (×). (After Bray and O'Keefe [15]. Reproduced with permission of the Society of Glass Technology.)



Note that $N_4$ does increase with added alkali as suggested by Warren. However, instead of stopping at about 16 mol % alkali, the $B_3 \rightarrow B_4$ conversion appears to continue right up to about $N_4 = 0.45$ and only decreases thereafter, approaching zero at around x = 70 mol %. Although this new experimental evidence confirmed the general idea of coordination changes of the network-forming cations in glass, it did suggest that the anomalous behavior of properties around 16 mol % added alkali had little to do with this conversion. One needed to look into other causes for the origin of the boron anomaly. More recent (perhaps more precise) measurements (16) of the expansion coefficient and the viscosity indicate that the property anomalies occur over a much wider range of composition, *viz.*, from about 13% to as high as 30% (instead of the previously thought narrow range around 16%). The proposed explanation currently for the boron anomaly is to regard the anomaly as a manifestation of the various atomic groups (Fig. 5-19) in which boron may be found as a function of the various alkali additions (Fig. 5-20).

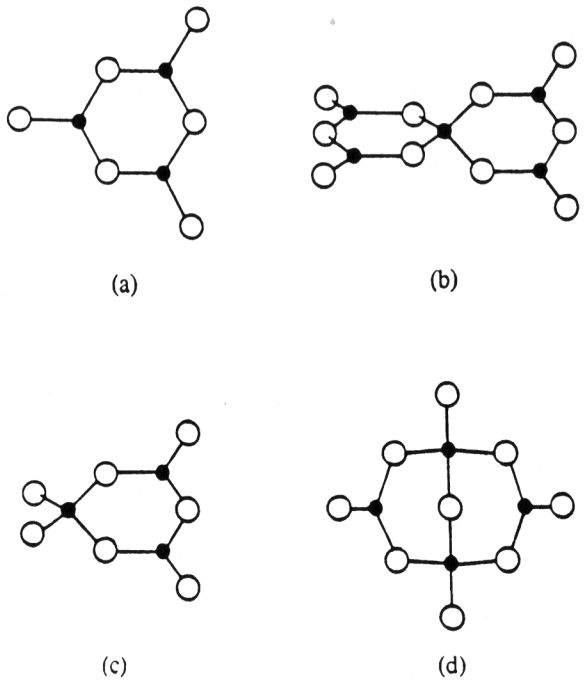


**Figure 5-19.** The various borate groups postulated to exist in alkali borate glasses having less than 34 mol % alkali. (a) The boroxol group. (b) The pentaborate group. (c) The triborate group. (d) The diborate group.

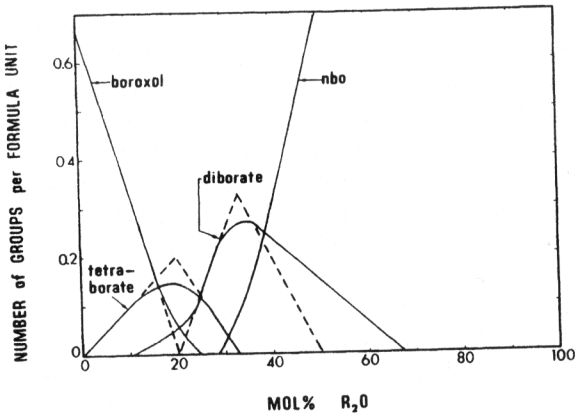


**Figure 5-20.** Structural models for alkali borate glasses. Note that the boroxol units disappear rapidly with alkali addition, giving rise to diborate units around 20 mol % alkali. (After Ref. 16. Reproduced with permission of the American Ceramic Society.)

If we express the molecular composition of the alkali borate glass as $RM_2O{\cdot}B_2O_3$, where $R = x/(1-x)$, then $N_4 = R$, and $f_{NBO} = 0$ up to $R = 0.5$. When $R > 0.5$, $N_4$ can be estimated by using Gupta's approximate relation (17)

$$N_4 = (3 - R)/5. \tag{5.3}$$

To calculate structural configurations in the alkali borates, one first needs to compute $R$. The computation of $N_4$ is then carried out. Finally, the $f_{NBO}$ is calculated by any leftover alkalis.

*Example 1*: Calculate the structural configurations in $20\,Na_2O{\cdot}80B_2O_3$ (mol %) glass.

We note that $R = 20/80 = 0.25$, which is less than 0.5.
Hence, $N_4 = R = 0.25$ and $f_{NBO} = 0$. Also, $N_3 = 1 - N_4 = 0.75$.
Average coordination number of boron $= 3 \times 0.75 + 4 \times 0.25 = 3.25$.

*Example 2*: Calculate the structural configurations in $40K_2O{\cdot}60B_2O_3$ (mol %) glass.

In this case, $R = 40/60 = 0.666$, which exceeds 0.5.
Hence, from Eq. (5.3), $N_4 = (3 - 0.666)/5 = 0.467$ (and $N_3 = 0.533$).
This yields $\#B_4 = 120 \times 0.467 \cong 56$.



Since one $B_4$ requires one $K^+$, this number of $B_4$ requires 56 $K^+$, leaving 24 $K^+$ to create 24 NBOs. Total number of oxygens are $40 + 180 = 220$.
Hence, $f_{NBO} = 24/220 = 0.11$.
Average coordination number of boron $= 3 \times 0.533 + 4 \times 0.467 \cong 3.47$.

## 5.8. Alkali Borosilicate Glasses

In alkali borosilicate glasses, $RM_2O{\cdot}KSiO_2{\cdot}B_2O_3$, there are two network formers: silicon and boron. The added alkali may associate either with silicon, creating an NBO as $SiO^-M^+$, or with boron, presumably converting a $B_3$ to a $B_4$ and creating no NBOs in the process. Again, using NMR techniques, it has been shown [18] that alkali prefers to associate with the boron as long as $R < 0.5$. Thereafter, the alkali distribution is partitioned between boron and silicon, creating NBOs depending upon the $K$ value. The behavior was confirmed using molecular dynamics calculations [9]. The variation of $N_4$ with $R$ and $K$ is shown in Fig. 5-21. Shown in Fig. 5-22 is a 3-D projection image for a borosilicate glass using MD techniques. The reader may be able to see the linked $BO_3$, $BO_4$, and $SiO_4$ groups by viewing a photocopy after adjusting the separation between the left and the right images under a portable stereographic viewer.

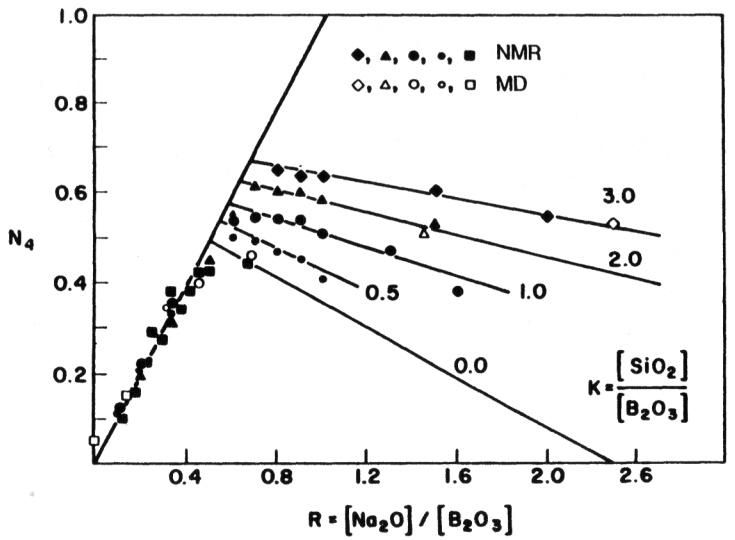


**Figure 5-21.** Fraction of tetrahedrally coordinated borons ($N_4$) as a function of mole $Na_2O/B_2O_3$ and $SiO_2/B_2O_3$ ratios. (After Ref. 9. Reproduced with permission of the American Ceramic Society.)

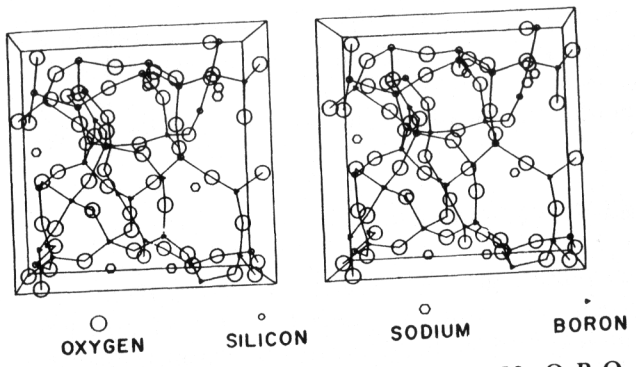


**Figure 5-22.** Stereographic image of a group of atoms in a $Na_2O$–$B_2O_3$–$SiO_2$ glass at 625 K. (After Ref. 9.)

## 5.9. Alkali Aluminosilicate Glasses

In alkali aluminosilicate glasses, the trivalent aluminum ion does not always act as a network former. The structural configurations depend upon the $[Al_2O_3/M_2O]$ ratio. Apparently, when $[Al_2O_3/M_2O] < 1$, the $Al^{3+}$ ion goes in as a network former having tetrahedral coordination. Like the $[BO_4]$ group, the excess unit negative charge on the $[AlO_4]$ group is satisfied by an alkali ion in the neighborhood. Thus, the addition of an aluminum ion to an alkali silicate glass removes one NBO. At $[Al_2O_3/M_2O] = 1$, there are no nonbridging oxygens in the structure. For further additions of $Al^{3+}$, i.e. when $[Al_2O_3/M_2O] > 1$, the $Al^{3+}$ ion enters the network as a modifier ion in octahedral coordination. Presumably three of the oxygens are nonbridging and three (already) bridging. This arrangement is shown in Fig. 5-23.

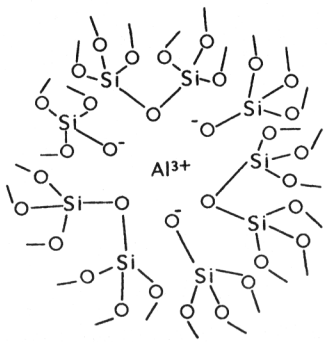


**Figure 5-23.** Suggested structure of an alkali aluminosilicate glass with $Al^{3+}$ as a network modifier showing octahedrally coordinated $Al^{3+}$.



According to Lacy [19], when $[Al_2O_3/M_2O] > 1$, the formation of $AlO_6$ groups is highly unlikely because of packing difficulties. He favors the formation of triclusters where an oxygen is shared between three tetrahedra: one $AlO_4$ and two $SiO_4$ or two $AlO_4$ and one $SiO_4$. (Note that oxygen bridging to three network formers violates Zachariasen's rules.) The first type of tricluster is electrically neutral; the second would require an associated alkali. These triclusters are shown in Fig. 5-24. In principle, the triclusters appear equivalent to an $Al^{3+}$ ion acting as a modifier ion and bonded to three nonbridging oxygens (shown in Fig. 5-24c). Thus, the basic question is whether an $Al^{3+}$ ion is surrounded by one (already) bridging oxygen or two or three. Experiments to understand the Al coordination sphere need to be carried out.

Because of the blocking effect of the Al ion in the interstices, electrical conductivity and the diffusion coefficient of the alkali ion decrease. In Fig. 5-25 is shown the activation energy for electrical conduction in $Na_2O$–$Al_2O_3$–$SiO_2$ glasses against the $Al_2O_3/M_2O$ ratio [20]. The increase in the activation energy at initial additions of alumina is attributed to the tightening of the structure due to the gradual disappearance of NBO. With further additions of alumina, the activation energy starts decreasing because of the looseness of bonding between the alkali ion and the $[AlO_4]^-$ group. When $[Al_2O_3/M_2O] > 1$, the activation energy starts increasing again because of the blocking effect of the octahedrally coordinated $Al^{+}$ ion in the interstices.

To calculate the structural configurations in the $M_2O{\cdot}Al_2O_3{\cdot}SiO_2$ glasses, one first needs to associate the alkali with available Al ions. Any residual alkalis then create nonbridging oxygens on the silicons. If the number of Al ions is greater than the number of alkali ions, then after all the available alkalis are associated with aluminum ions, each residual Al ion creates three NBO.

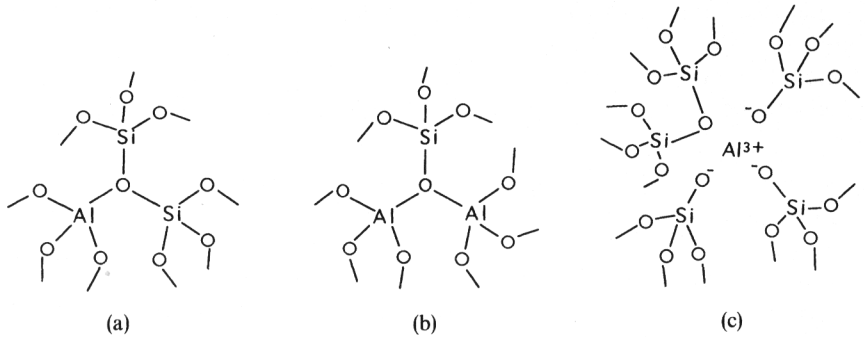


**Figure 5-24.** Tetrahedrally coordinated $Al^{3+}$ in tricluster arrangements (a) and (b) according to Lacy. Note that (c) is equivalent to (a).

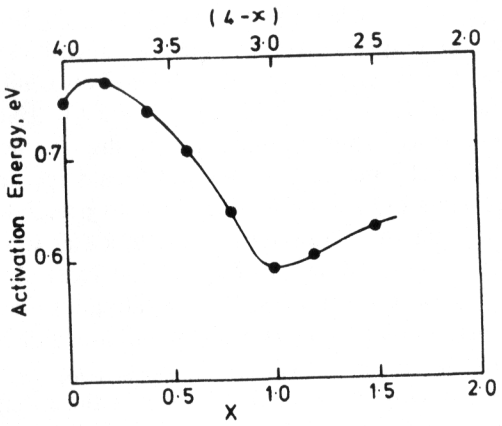


**Figure 5-25.** Effect of composition on the activation energy for dc conduction in the $Na_2O{\cdot}xAl_2O_3{\cdot}2(4\text{-}x)SiO_2$ glass system. (After Isard (20). Reproduced with permission of the Society of Glass Technology.)

*Example 1*: Calculate the structural configurations in a $15Na_2O{\cdot}10Al_2O_3{\cdot}75SiO_2$ glass.

In this case $[Al_2O_3/M_2O] < 1$; hence, $\#Al\square = 20$, which absorb 20 Na ions.
Remainder #Na ions = 10, which create 10 NBO. Hence, $f_{NBO} = 10/195$.
Total number of tetrahedra = 20 (for Al) + 75 (for Si) = 95.

*Example 2*: Calculate the structural configurations in a $20Na_2O{\cdot}20Al_2O_3{\cdot}60SiO_2$ glass.

In this case $[Al_2O_3/M_2O] = 1$; hence, $\#Al\square = 40$, which absorb 40 Na ions.
Remainder #Na ions = 0. Hence, $f_{NBO} = 0$.
Total number of tetrahedra = 40 (for Al) + 60 (for Si) = 100.

*Example 3*: Calculate the structural configurations in a $10Na_2O{\cdot}15Al_2O_3{\cdot}75SiO_2$ glass.

In this case $[Al_2O_3/M_2O] > 1$; hence, $\#Al\square = \#Na = 20$.
Remainder #Al ions (octahedral) = 10, which create 30 NBO.
Hence, $f_{NBO} = 30/205$.
Total number of tetrahedra = 20 (for Al) + 75 (for Si) = 95.



## 5.10. Lead, Bismuth, and Thallium Silicate or Borate Glasses

PbO can be present up to as much as 92 wt. % in lead silicate glasses, and perhaps up to 94% in borates. If Pb were present as network-modifier ions only, then the 92% PbO would be beyond the limit where all the $SiO_4$ tetrahedra are connected. Based upon XRD of $PbO{-}SiO_2$ glasses of up to 60 mol % (84.6 wt. %) PbO, Bair [21] suggested (by extrapolation) that for the $2PbO{\cdot}SiO_2$ composition all the $SiO_4$ tetrahedra must be connected to each other via a Pb atom, thus allowing a glass network-forming role for Pb where all the oxygens are bridging and connected to one Si and one Pb atom. Refined XRD work [22] later on showed that the first Pb–Pb distance was 3.9 Å, and the coordination of Pb around Pb varied between 6 and 9. A possible structure for $2PbO{\cdot}SiO_2$ is shown in Fig. 5-26a. Note that, because of the 2-coordination of Pb, the structure contains substantially large holes in which presumably more PbO could be accommodated, if needed. NMR work, however, has revealed the presence of $PbO_4$ pyramids where Pb forms the vertex. Current belief is that, as in crystalline PbO, high-lead glasses may

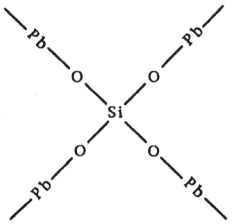


(a)

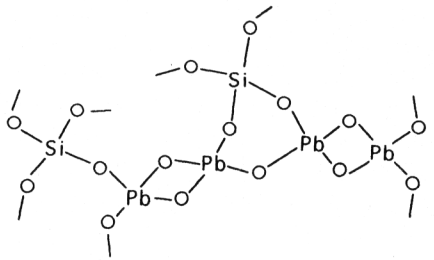


(b)

**Figure 5-26.** Structure of lead silicate glasses showing (a) two-coordinated Pb, (b) tetrahedrally coordinated Pb. (After Mydler *et al.* [22]. Redrawn with permission of the Society of Glass Technology.)

have Pb–O–Pb bonds in the form of twisted $PbO_4$ pyramids (Fig. 5-26b). Apparently, four Pb–O distances are 2.3 Å and four other Pb–O distances are 4.3 Å: the asymmetry of the pyramids contributes towards randomness.

As in the $PbO–SiO_2$ glasses, glass formation in $Bi_2O_3–SiO_2$ and $Tl_2O–SiO_2$ glasses can occur up to very high "modifier" content. Because the $Bi^{3+}$ and the $Tl^+$ ions are very large, they are highly polarizable. The high polarizability apparently leads to a high degree of asymmetry in the cation–oxygen polyhedra, and perhaps helps glass formation.

## 5.11. Phosphate Glasses

Phosphorus is a network-forming element. However, only $P_2O_5$ is known to form a glass. All three allotropic forms of $P_2O_5$ (hexagonal H, orthorhombic O, and tetragonal T) can form glasses after melting and cooling. The H form slowly converts to the O form around 380°C, which itself is metastable with respect to the T form from the melting point (580°C) down to 70°C. Because of the slow conversion to the T form, the properties of glass such as the viscosity and refractive index depend upon the parent crystalline form, the melting time, and the cooling rate. In both the crystals and the glasses, the basic unit of structure is the $PO_4$ tetrahedron. Because P is a pentavalent ion, one oxygen from each tetrahedron remains nonbridging to satisfy charge neutrality of the tetrahedron (Fig. 5-27). In this respect, $P_2O_5$ differs from $SiO_2$.

Because of the presence of the nonbridging oxygen, which can act as a terminator, $P_2O_5$-containing glasses can form isolated ring (cyclic) molecules. It is believed that the melt obtained from the hexagonal form initially contains isolated $P_4O_{10}$ molecules (Fig. 5-27b), which gradually link up to form larger-sized (cyclic) molecules, then linear-chain and finally layered-sheet structures. In $P_2O_5$, the connections are made only at three corners (unlike $SiO_2$, where all four corners are connected) (Fig. 5-27a); hence, the $P_2O_5$ glass is significantly less rigid (or is more fluid) compared to $SiO_2$ glass. Presumably, like the $B_2O_3$ glass, the $P_2O_5$ glass in the sheet form consists of layers of oxygen polyhedra with weak van der Waals attraction between the layers. The rigidity of the structure is increased by the addition of alkalis or alkaline earths. The extent of glass formation in alkali and alkaline earth binary phosphates is shown in Table 5-3 and is generally larger than in the silicates or the borates. The range is larger when, for instance, mixed alkalis are present. It is believed that the ring molecules are broken by the modifier ions to form linear phosphate chains with varying chain lengths depending upon the modifier ion/phosphorus ratio. For instance, in



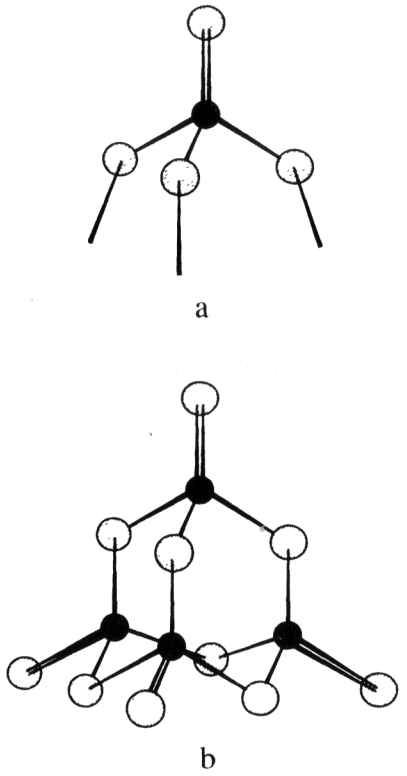


**Figure 5-27.** Structures of (a) $PO_4$ and (b) $P_4O_{10}$ molecules. Darker-shaded circles represent P.

$Na_2O–P_2O_5$ glasses with a Na/P ratio exceeding 1, linear chains of the general formula $Na_{n+2}P_nO_{3n+1}$ and cyclic chains of the general formula $(NaPO_3)_n$ are found. Some examples of linear chain configurations in alkali and alkaline earth phosphates are shown in Fig. 5-28.

The measurement of chain lengths has been accomplished by dissolving the glass in water and using paper chromatography techniques, notably by Westman [23]. (It has been shown that the dissolution process in water does not create or destroy the polymeric structure already present in the glass.) The distribution of chain lengths in various sodium phosphate glasses with $Na/P \geq 1$ is shown in Fig. 5-29. The percentage of total phosphorus present in linear chains with various values of $n$ are plotted against the parameter $n_{av}$ (=number average chain length), and $T$ ($=100/n_{av}$, the number of molecules per 100 P atoms). The numbers on the curves give the values of

**Table 5-3.** Regions of Glass Formation in Binary Phosphate Systems[a]

| Modifier | Maximum percentage of modifier (mole per cent) | |
|---|---|---|
| | Elyard *et al.*[b] | Imaoka[c] |
| $K_2O$ | — | 47 |
| $Na_2O$ | — | 60 |
| $Li_2O$ | — | 60 |
| BaO | 57 | 58 |
| SrO | 56 | 56 |
| CaO | 58 | 56 |
| MgO | 65 | 60 |
| BeO | — | 66 |
| $Ag_2O$ | — | 66 |
| $Tl_2O$ | — | 50 |
| ZnO | 71 | 64 |
| CdO | 66 | 57 |
| PbO | 66 | 62 |

[a] After Rawson.

[b] Melted on scale of approximately 20 mg on electrically heated platinum alloy wire. Melt quenched by switching off the heating current. C. A. Elyard, P. L. Baynton, and H. Rawson, *Glastech. Ber.*, 32K, V, 36–43 (1960).

[c] Melted on scale of 1–3 g in platinum crucible. Melt cooled in the crucible. M. Imaoka, in "Advances in Glass Technology, Part I", pp. 149–164, Plenum Press, New York (1962).

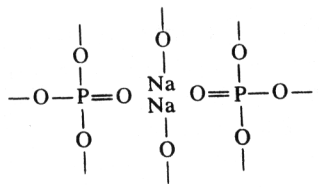


**Figure 5-28.** Crosslinking of $P_2O_5$ by (a) alkali and (b) alkaline earth oxides.



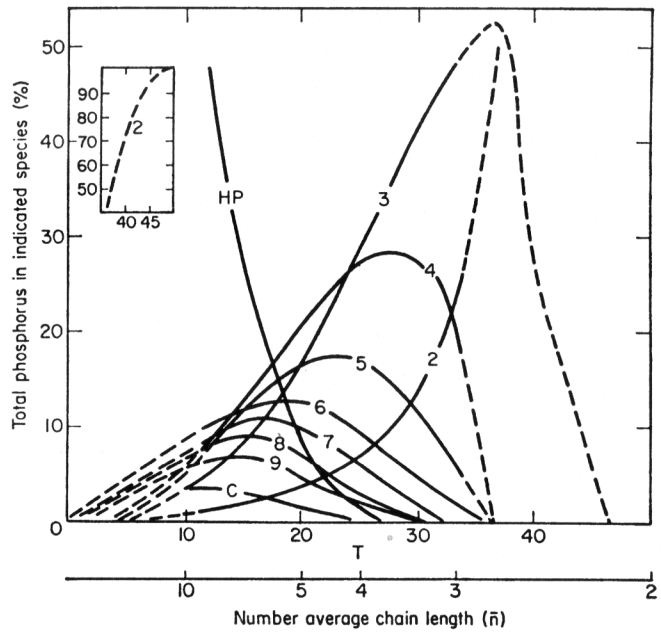


**Figure 5-29.** Constitution of sodium phosphate glasses. HP = hypolyphosphite; C = total cyclic phosphates. Inset shows the extension of the pyrophosphate curve ($n = 2$). Dashed lines on the right are based on results for rapidly flame-fused beads. Dashed lines on the left are extrapolations. (After Westman (23). Reproduced with permission of Butterworth-Heinemann Ltd., Oxford.)

$n$ from 2 to 9. Curve HP ("hypolyphosphate") gives the percentage in linear molecules with $n > 9$, and the curve C is the percentage in cyclic molecules. If the number of cyclic molecules is ignored, then $n_{av}$ may be calculated using the formula $n_{av} = 2/[(Na/P) - 1]$, which shows that the composition $Na_2O{\cdot}P_2O_5$ with Na:P = 1:1 has essentially a single infinite-chain-length molecule ($n_{av} = \infty$).

The charge compensation for the $PO_4$ tetrahedron can be accomplished exactly by replacing one pentavalent P by one trivalent Al or B. Thus, the structure of $AlPO_4$ is isomorphic to $SiO_2$ (written as $SiSiO_4$). In fact, in the crystalline form, analogous allotropic forms of $AlPO_4$ exist for all allotropic forms of silica (including high and low forms). Yet, $AlPO_4$ can only be brought to glassy state by vapor phase condensation. The reasons for this anomaly (relative to silica) are not clearly understood. It is suggested [24] that with the addition of $Al_2O_3$ to $P_2O_5$, the size of the tetrahedral $AlO_4$–$PO_4$ clusters continue to grow; however, full connectivity is still not obtained even at the stoichiometric $AlPO_4$ composition, allowing structural rearrangement, and thus crystallization, to occur. Experimental problems in

the melting of $AlPO_4$ are augmented because of the rapid volatilization of $P_2O_5$.

## 5.12. Other Oxide Glasses

Among other oxide glasses, only $GeO_2$ is known to form a glass by normal cooling of a melt. The glass has a tetrahedral quartzlike structure, rather than the more open cristobalite-like structure of silica glass. This presumably results from the fact that Ge/O radius ratio is 0.414, which is on the border between tetrahedral and octahedral structures. Neutron diffraction studies show that the primary Ge–O bond is 1.73 Å (about 8% larger than the Si–O bond). Other bond distances are O–O = 2.83 Å, Ge–Ge = 3.45 Å; the average Ge–O–Ge bond angle is 133° (compared to about 144° for the Si–O–Si bond angle in silica glass).

Upon the addition of modifier alkalis, the coordination number of Ge changes from 4 to 6. As shown by Kamiya and Sakka (25), the conversion continues to occur up to about 35% $GeO_6$ at around 30% added alkali. Thereafter, a sharp decrease is observed (Fig. 5-30). Not all of the oxygens in the $GeO_6$ group are bridging.

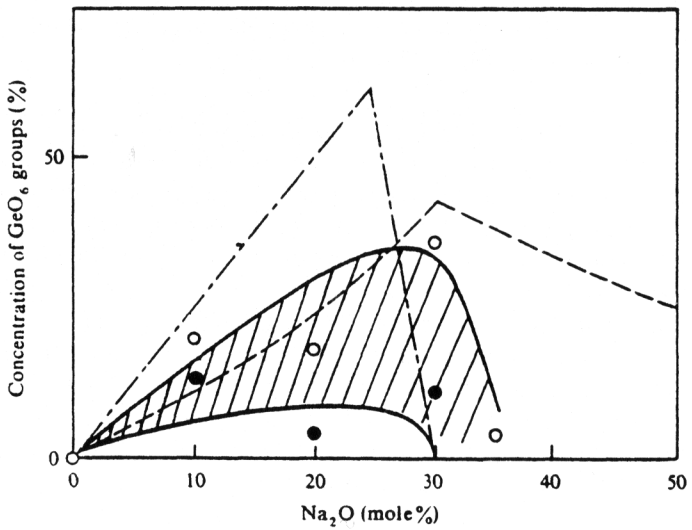


**Figure 5-30.** Concentration of $GeO_6$ groups as a function of $Na_2O$. Open circles and filled circles are calculated upper and lower limits. (After Kamiya and Sakka [25]. Reproduced with permission of the Society of Glass Technology.)



$Al_2O_3$, $As_2O_3$, $Sb_2O_3$, $Bi_2O_3$, $V_2O_5$, $TiO_2$, $TeO_2$, etc., are not known to form glasses readily. However, some such as $As_2O_3$, $Sb_2O_3$, and $V_2O_5$ have been claimed to form glasses by vapor-phase condensation, or by splat-cooling techniques. Many binary glasses that include a large amount of these oxides can be formed, particularly with alkalis, alkaline earths, PbO, and other glass network formers. For example, Table 5-4 shows the glass formation range in binary tellurite glasses. The coordination number of Al in aluminate glasses is thought to be 4. However, such studies are not conclusive. In arsenates, antimoniates, and bismuthates, it has been found that the primary polyhedra are pyramids of $MO_3$ with M slightly out of the oxygen triangular plane (much as in $B_2O_3$). In vanadates, the vanadium is present as $VO_4$ tetrahedra having three bridging oxygens and one doubly bonded nonbridging oxygen (as in $PO_4$). In tellurites, $Te^{4+}$ ion may occur in three or four coordinated structures.

**Table 5-4.** Range of Glass Formation in Tellurite Systems[a,b]

| Metal oxide | Range (mol %) |
|---|---|
| $Li_2O$ | 12.2–34.9 |
| $Na_2O$ | 5.5–37.8 |
| $K_2O$ | 6.5–19.5 |
| $Rb_2O$ | 5.6–21.0 |
| BeO | 15–27 |
| MgO | 11–35 |
| CaO | — |
| SrO | 9.2–13.1 |
| BaO | 8.0–35.7 |
| ZnO | 17.3–37.2 |
| $Al_2O_3$ | 7.6–16.8 |
| $Tl_2O$ | 13.0–38.4 |
| PbO | 12.8–22.6 |
| $Nb_2O_5$ | 2.2–24.0 |
| $Ta_2O_5$ | 1.4–15.3 |
| $WO_3$ | 8.5–44 |
| $La_2O_3$ | 4.5–9.5 |
| $TiO_2$ | 6.2–18.9 |
| $ThO_2$ | 5.2–11.0 |

[a] From W. Vogel, H. Bürger, B. Müller, G. Zerge, W. Müller, and K. Fortel, *Silikattechnik*, **25**(6), 205–209 (1974).

[b] 20–100 g, cooled at 8–10°C/s through transformation.

## 5.13. Amorphous Silicon and Germanium

In amorphous silicon (abbreviated *a*-Si) and *a*-Ge, the local atomic coordination number = 4 (from the "8-*N*" rule, Section 3.1.4). The structure of these amorphous solids is hence believed to be a continuous random network (CRN) of tetrahedrally bonded atoms. The structure is similar to the diamond lattice in that each atom is four-coordinated, bond lengths are constant, and there are no dangling bonds. However, in contrast to the diamond structure, there presumably is a spread of bond angles, and of course, there is no long-range periodicity.

Polk (26) was the first to attempt to construct a model of *a*-Si that observed the preceding criteria. Metal rods of equal length representing the bonds snapped into a plastic section representing the atom. The plastic section

**Figure 5-31.** Polk model for the structure of *a*-Si. Five-membered rings may be seen at the top (atoms 10, 11, 13, 14, 15) and lower right (atoms 3, 4, 5, 12, 7). A six-membered ring in "chair" configuration is on edge at the right (atoms 4, 5, 6, 11, 12, 13). "Boat"-configured six-membered rings are at the left (atoms 1, 2, 10, 15, 8, 9 and atoms 7, 3, 2, 8, 15, 10).



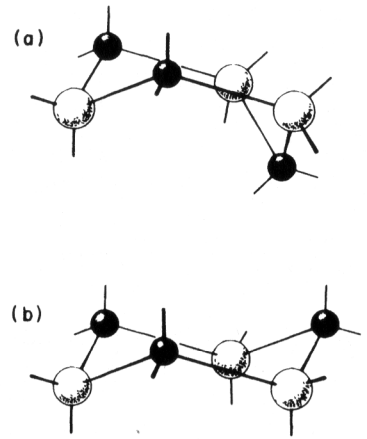


**Figure 5-32.** (a) "Boat" and "chair" configurations of six-membered rings.

could be bent somewhat, allowing slight variation in the tetrahedral angles. Polk showed that for the fixed equal bond lengths, the variation in $\Delta\theta$ in the tetrahedral angle (109° 28′) was only about 9°. A small portion of his 440-atom model is shown in Fig. 5-31.

Whereas the shortest of the rings in crystalline silicon are six-membered, the shortest in the Polk model was five-membered. The six-membered rings in the diamond structure all have the "chair" type of configuration (Fig. 5-32b) with staggered (60°) dihedral angles (Fig. 5-33b). In the crystalline wurtzite structure, one-quarter of the six-membered rings have the "chair" configuration and three-quarters have the "boat" configuration (Fig. 5-32a). In the latter, four dihedral angles are staggered, and two are eclipsed (Fig. 5-33a). In the Polk model, the dihedral angles varied as a smooth increasing function from 0° to 60°, indicating the presence of both the chair and boat configurations. The calculated and measured [27] RDFs of *a*-Si are compared in Fig. 5-34. Note the sharpness of the bond length in the Polk model and the apparent disagreement with the measured RDF. One would tend to argue that bond lengths presumably vary more than was assumed by Polk. As a result, the medium-range order and, in particular, the ring statistics of the Polk model are clearly wrong.

In fact, the difficulty lies more in terms of the constraints applied in building stick-and-ball models. Using a Keating-type potential (involving bond-stretching and bond-bending distortions, similar to Eq. (3.3)) in a computer model of as many as 519 atoms, Steinhardt *et al.* [28] obtained an RDF for *a*-Ge that was then relaxed for vibrational, instrumental, and analytical broadening. The resultant RDF was found to be in very good

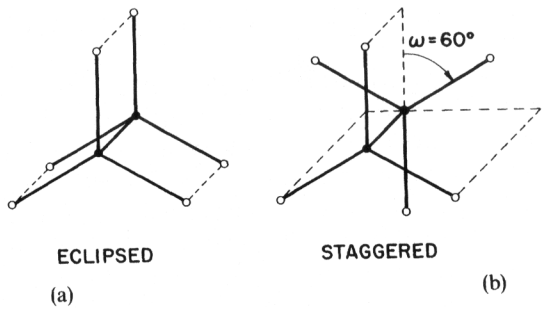


**Figure 5-33.** The (a) eclipsed and (b) staggered bond orientations in tetrahedrally bonded structures.

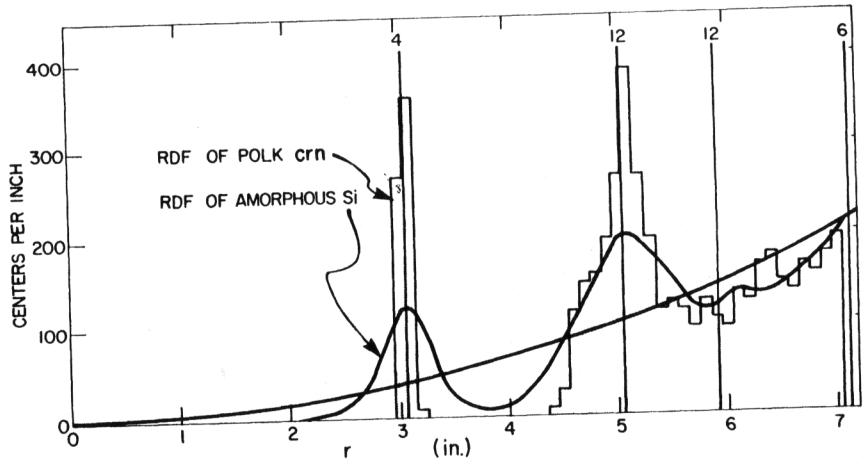


**Figure 5-34.** Comparison of measured RDF of *a*-Si with that of the Polk CRN model. (Note that the experimental RDF distance was scaled up by a factor of $10^8$ to correspond with the model dimensions in inches.) (After Moss and Graczyk [27]. Reproduced with permission of Elsevier Science Publishers.)

agreement with one measured experimentally (Fig. 5-35). Steinhardt *et al.* further showed that the introduction of 1% variation in bond lengths allowed the angular variation to be reduced to 7%, which brought the amorphous structures energetically closer to the crystalline structures while still maintaining good agreement of the RDFs. (There may still be some room to argue that agreement between the Steinhardt *et al.* calculation and the experimental data for the Ge–GeII peaks is far from being excellent.)

On the whole, the Polk model for the structure of amorphous semi-



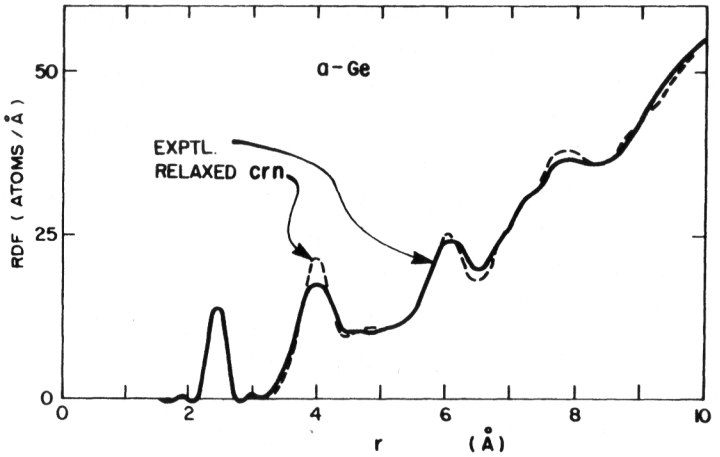


**Figure 5-35.** Comparison of measured RDF of *a*-Ge with that of the relaxed CRN model. (After Steinhardt *et al* [28]. Reproduced with permission of Elsevier Science Publishers.)

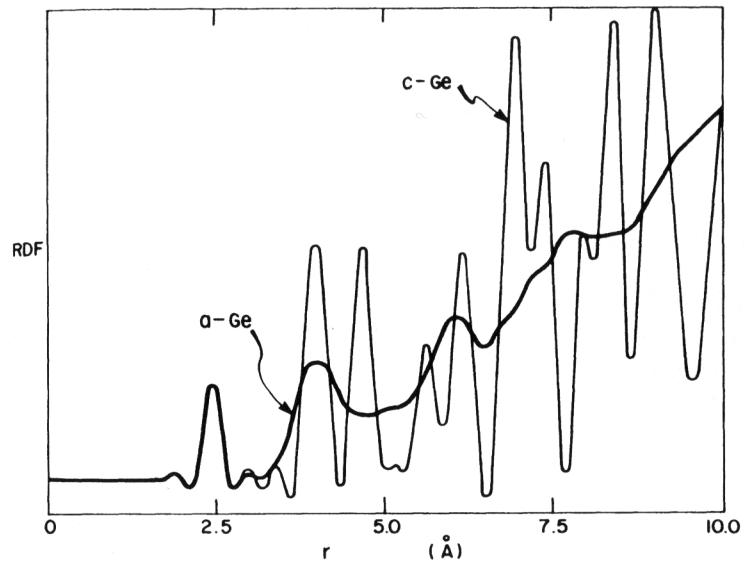


**Figure 5-36.** Comparison of x-ray derived RDFs of *a*- and *c*-Ge. (After R. J. Temkin, W. Paul, and G. A. N. Connell, *Adv. Phys.* **22**, 581 (1973). Reproduced with permission of Taylor & Francis, Inc.)

conductors appeared successful. The most interesting feature was the third near-neighbor peak in the crystal, which was completely absent in the amorphous material (e.g., see Fig. 5-36 for Ge). More importantly, though, it brought out the following:

1. It is possible to arrange atoms in a fairly tight short-range order, but not have long-range order typical of crystals.
2. Stick-and-ball models generally do not represent the medium-range order well enough to give accurate ring statistics.
3. Computer simulations need to be carried out carefully to include the different relaxation procedures; otherwise, the comparison of the calculated RDF with experimentally measured RDF is not meaningful. In colloquial terms, it is called "GIGO" or "garbage in, garbage out."

One should bear in mind that the Polk model applies to purely covalent solids. In many ways, the structure is quite simple indeed (in fact, the simplest of all considered so far). Next, we consider an even simpler structure: that of glassy metals, where there are no covalent bonds, no fixed coordination, and the metallic bond allows more variation on the bond distance.

## 5.14. Glassy Metals

Glass formation in metallic systems occurs in four basic binary systems: (a) the transition metal–metalloid (abbreviated as T-M) system; (b) the early and late transition metals (TE, TL) system; (c) the alkaline earth (AE) with rare earths (RE) and simple metals (S) system; and (d) the transition metal–actinides (T-AC) system. Table 5-5 is a summary of the basic binary systems. Of these, the first system, where the content of the transition metal is generally about 70–80% and the metalloid up to about 30%, is perhaps the most studied one.

Models to describe the structure of the glassy metals generally fall within one of the four classes: microcrystallites, random network, dense random packing of spheres, and random packing of trigonal prisms. The first two are quite like the ones proposed for oxide systems, are based on XRD data, and obviously suffer from like criticism. The broadening of x-ray peaks could be fitted to a crystallite size, but such crystallites would often have to be quite small to be meaningful as "ordered" clusters. As in the case of oxide glasses, the random network model fits mostly single-component amorphous



**Table 5-5.** Binary Glass-Forming Metallic Systems

| Group | Class[a] | Typical composition of glasses | Most stable intermetallic compounds |
|---|---|---|---|
| a | T–M | $Pd_{80}Si_{20}$ | $Pd_3Si$, $Fe_3P$ (cementite) |
| | | $Ni_{80}P_{20}$ | $Pd_2Si$, $Fe_2P$ |
| | | $Fe_{40}Ni_{40}P_{14}B_6$ (Metglas 2826) | |
| b | TE–TL | $Nb_{60}Ni_{40}$ | "NbNi" disordered phase |
| | | $W_{45}Fe_{55}$ | $Fe_7W_6$ phase |
| | | $Zr_{76}Fe_{24}$ | |
| | TL–RE | $Co_{33}Gd_{67}$ | $CdCo_2$ Laves phase |
| | | $Ni_{30}Gd_{70}$ | $GdCo_5$, $Gd_2Co_{17}$ } Frank–Kasper phase |
| c | AE–AE | $Ca_{67}Mg_{33}$ | $CaMg_2$ Laves phase |
| | AE–S | $Mg_{70}Zn_{30}$ | $MgZn_2$ Laves phase |
| | AE–T | $Ca_{65}Pd_{35}$ | $CaPd_2$ Laves phase |
| | S–RE | $Al_{30}La_{70}$ | $LaAl_2$ Laves phase |
| d | AC–T | $U_{70}Cr_{30}$ | |

[a] T = transition metal; M = metalloid; TE = early transition metal; TL = late transition metal; RE = rare earth; AE = alkaline earth; S = simple metal; AC-actinide.

solids (*a*-Si and *a*-Ge, discussed earlier). The third and the fourth models describe the structure of most of the glassy metal systems equally well, and they are worth considering here in more detail.

The concept of **dense random packing (DRP)**, sometimes called **random close packing (RCP)**, of single-sized hard spheres to describe liquid structures had been advanced by Bernal [29] and was adopted later for the description of glassy metal structures. The idea is simple conceptually: take monosized hard spheres and place them in a flexible bag; squeeze on the bag till the volume does not shrink significantly. The locations of the centers of the spheres simulate a glassy metal. These simulations have now been tried using 7,934 ball bearings by Finney [30], and as computer experiments by Bennett [31]. The RDFs measured from these simulations are generally in good agreement with those measured using XRD (Fig. 5-37). The packing fraction obtained in both the physical models is about 0.64, which is less than the closest packing fraction (0.74) of the fcc and the hcp structures. This difference in the packing fraction is undoubtedly due to the presence of holes in the amorphous structures that are large enough to accommodate a smaller hard sphere (but not enough for another equisized hard sphere). The centers of the spheres themselves are vertices of one of five types of polyhedra (Fig. 5-38) (allowing for some distortion of the edges). The holes enclosed by the

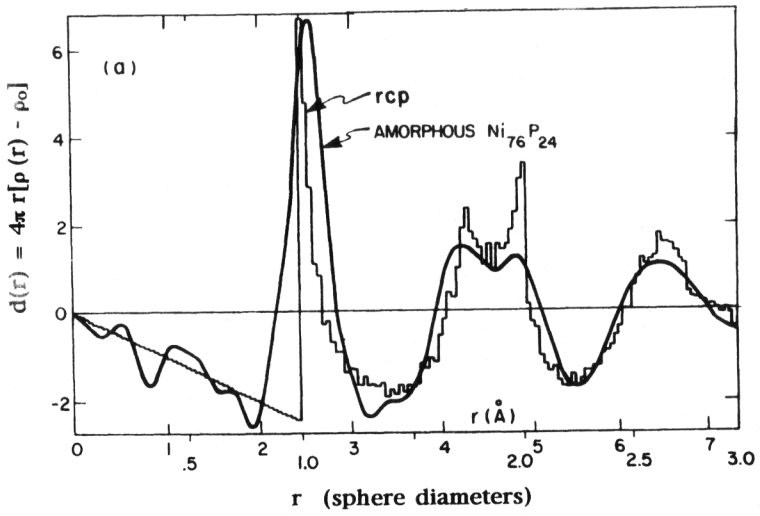


**Figure 5-37.** (a) Comparison of the differential correlation function $d(r)$ for Finney's DRP of monosized spheres and the experimental curve for $a$-$Ni_{76}P_{24}$. Inset (b) the origin of the double peak at second coordination. (After G. S. Cargill, *Sol. St. Phys.* **30**, 227 (1975).)

polyhedra are called **Bernal's canonical holes**. The canonical holes share faces and fill the space. Of the five canonical polyhedra, the smallest, i.e., the tetrahedron, occurs most frequently; there are about 2.9 tetrahedral holes per sphere. This is about 25 times more the next most frequent [32] (the trigonal prism and the tetragonal dodecahedron).

Another way of filling the space in the DRP structures would be through **Wigner-Seitz cells**, which in disordered systems are actually *Voronoi polyhedra* (Fig. 5-39). These are the polyhedra whose faces are the planes perpendicular to, and passing through the midpoint of, the lines joining the sphere centers. (About 40% of the faces are pentagons.) If a large number of fresh peas were placed in a pot, shaken well till volume did not decrease much further, water was added to cover them, and a sufficiently heavy lid



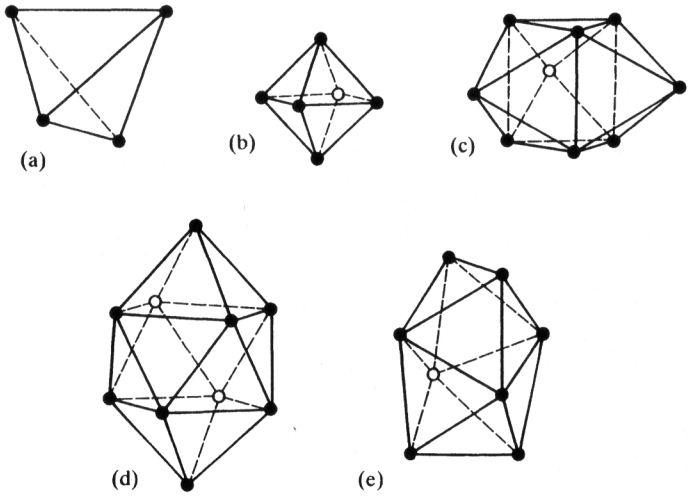


**Figure 5-38.** The "canonical holes" of Bernal. (a) Tetrahedron. (b) Octahedron. (c) Trigonal prism (shown capped with half-octahedra at each of the three rectangular faces). (d) Archimedean anti-prism (shown capped with half-octahedra on the bottom and the top faces). (e) Tetragonal dodecahedron.

closed off the volume (without any air above the peas), then the peas would essentially dilate into Voronoi polyhedra (experiment of botanist Stephen Hales, 1727).

The **random trigonal prisms packing (TPP)** model was suggested by Gaskell [32B] to describe the structure of the transition metal–metalloid glasses. Apparently, $MT_6$ trigonal prisms found in $T_3M$ crystalline alloys appear to persist in glasses of close compositions such as $T_4M$. The T atoms are at the apices of the trigonal prism (the $T_I$ sites), and the M atom is at the center of the prism (Fig. 5-40a). In the cementite ($Fe_3C$) structure, where the radius ratio of M to T is small, there are three other T atoms that surround the M atom on the equatorial plane (placed in the octahedral site of the rectangle ABED), but at a larger distance from M (the $T_{II}$ sites). The location of the second prism is obtained by rotating the first prism 215° clockwise about the axis AB (Fig. 5-40b). The second prism then shares the edge AB (two $T_I$ sites) with the first prism, and G (a $T_{II}$ site) to make up its triangular base. The small radius ratio allows the trigonal prisms to have little distortion; as a result, the $M–T_{II}$ distances are significantly larger than the $M–T_I$ distances. On the other hand, when the M to T radius ratio is large, as in the $Fe_3P$ structure, the $T_{II}$ sites are placed in the tetrahedral site above the ABC triangle, and again the second prism shares AB (two $T_I$ sites) and G (one $T_{II}$ site); see Fig. 5-40c. Because of the large size of the metalloid

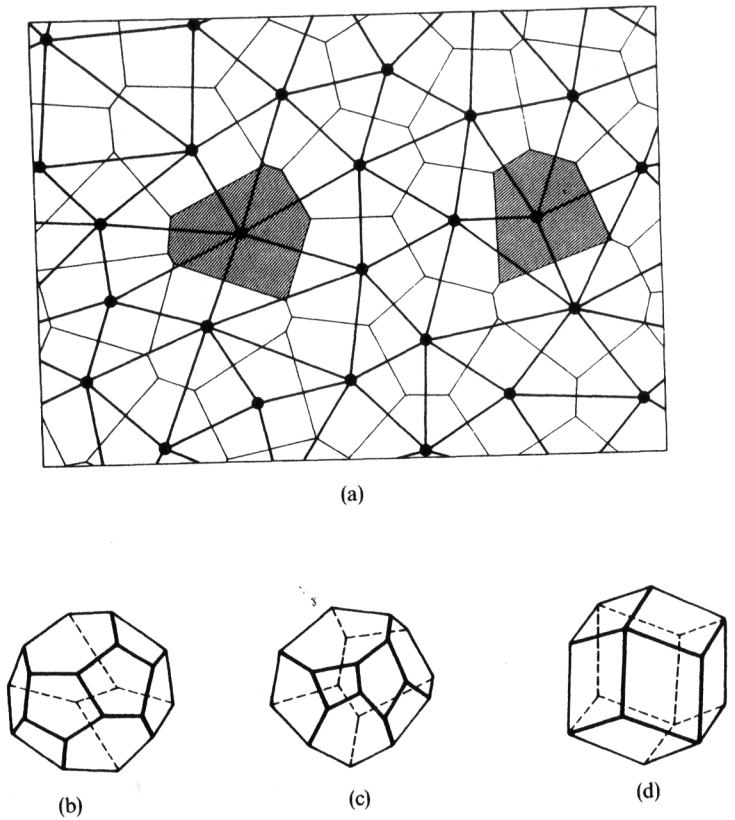

(a)



(b) (c) (d)

**Figure 5-39.** (a) 2-D projection of the spaces (Voronoi polyhedra or Wigner–Seitz cells) occupied by dense random packing of atoms. Note that the atom centers are joined, and the perpendicular bisector planes are constructed. The different planes are the faces of the Voronoi polyhedra. (After R. Zallen, *The Physics of Amorphous Solids*, Fig. 2.5, p. 47. Wiley & Sons, New York, 1983. Reproduced with permission of the publishers.) (b) and (c) Two possible shapes of the Voronoi polyhedron when peas are allowed to swell to occupy space. Note the predominance of pentagonal faces. (d) Rhombic dodecahedron cell of the ordered cubic close packing.

atom, the M–$T_I$ distances are larger in the $Fe_3P$ structure than in the cementite structure, and the M–$T_{II}$ distances are not much greater than the M–$T_I$ distances. Randomness in the sharing of edges in both these motifs then allows varying chain or 3-D structures over a variety of composition ranges. For instance, when on an average two edges are shared, the composition would be $T_4M$.



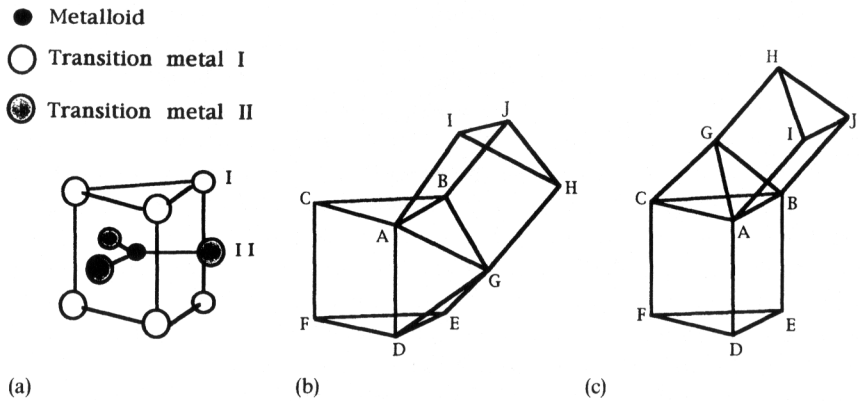


(a) (b) (c)

**Figure 5-40.** (a) Trigonal prismatic packing of transition metals around a metalloid atom. (b) Edge-sharing arrangements in the $Fe_3C$ (cementite) structure. (c) Edge-sharing arrangements in the $Fe_3P$ structure. Note the distance between the metalloid atom M and the second nearest neighbor transition metal ($T_{II}$) is smaller here than in (b).

## 5.15. Chalcogenide and Chalcohalide Glasses

The chalcogen elements (S, Se, and Te) can form glasses by themselves upon cooling from a melt. Glasses made by combining chalcogen elements with group IV and V elements are termed chalcogenides. When combined with the halogen group of elements, the glasses are called chalcohalides. Glasses consist of disordered rings (molecules), chains, sheets, and three-dimensional networks. The bonding is generally covalent, with weak van der Waals attraction between the molecules, chains, etc. The coordination number of various elements in the chalcogenide glasses is given by the "8-$N$" rule, where $n$ is the number of the outer shell electrons (see Section 3.1.4). Thus, the coordination number of the chalcogen elements is 2; that for As and Sb is 3, and for Ge it is 4. In a chalcogenide/chalcohalide glass, the average coordination number, $\langle m \rangle$, may be defined as the atom-averaged coordination number of the constituent atoms. Thus, a 28Ge·12Sb·60Se glass has an $\langle m \rangle$ value of $[\{28(4) + 12(3) + 60(2)\}/100] = 2.68$. The pure element chalcogen glasses ($\langle m \rangle = 2.0$) are essentially chains that polymerize to varying lengths. For instance, S melts at 115°C to a liquid containing roughly an $S_8$ ring structure. Upon further heating, the rings open up and polymerize to spirals that may have as many as $10^6$ atoms. This structure continues into the glassy form when the stiffened liquid is rapidly cooled. Apparently, the $Se_8$ rings are easier to break up, and hence, a pure Se glass is easier to obtain.

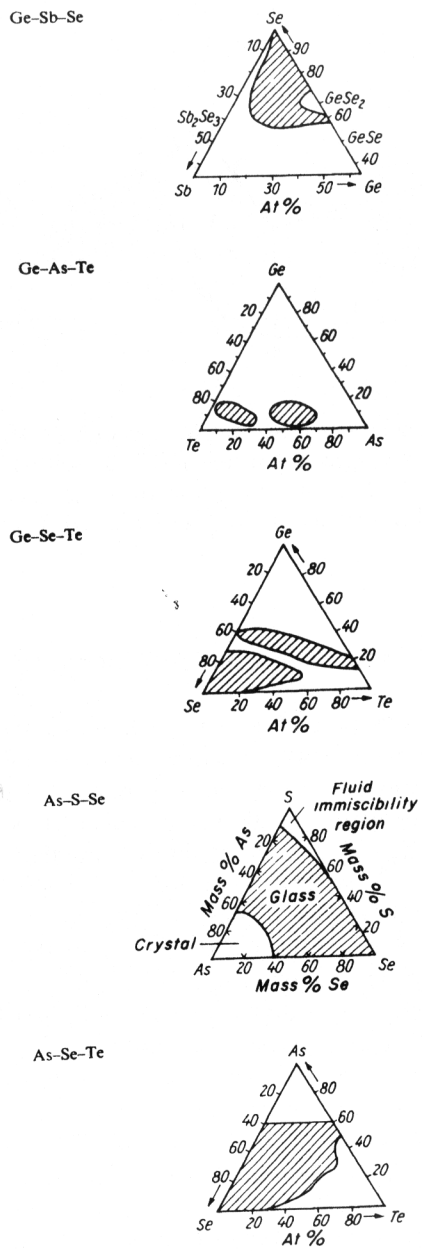


**Figure 5-41.** Glass formation region shown shaded in the Ge-Sb/As-S/Te ternary diagrams. (From W. Vogel, *Chemistry of Glass*, pp. 184–190. Amer. Ceram. Soc., 1985. Reproduced with permission of the publisher.)



Pure Te glass, on the other hand, is not very readily obtained and requires very rapid quenching from just above the melting point of Te crystal.

*The addition of group IV and V elements causes the chains to begin to crosslink* because of the increased coordination requirement (4 for group IV and 3 for group V). Since the bonds are covalent, the crosslinking reduces the freedom for disorder. Nevertheless, glass formation is possible over a large range of compositions with various elements. Binary glasses such as As–Se, As–S, Ge–Se, and Sb–Te are not too difficult to obtain. Likewise, large composition ranges in ternary and other multielements can be brought to the glassy state. For instance, the glass formation range is shown shaded on the Ge–Sb–Se, Ge–As–Se, and Si–As–Te ternary diagrams in Fig. 5-41. At low crosslink densities, Ge acts as if it ended four selenium chains; As ends three chains. A 2-D projection ("pancaked version") of one such structure is shown in Fig. 5-42. At moderate to high crosslink densities, the question of crosslink atom bonding is not well understood. On each side of the ternaries, binary crystalline stoichiometric compounds exist. Tie lines joining these binary compounds are called "stoichiometric tie lines." The structure of the glasses changes radically as one crosses these tie lines. Some researchers believe that crosslink atoms can bond randomly (**random covalent network** or the **RCN** model). In other words, in a binary chalcogenide glass $A_{1-x}B_x$, the probability of A–A, A–B, and B–B bonds is determined by random statistics. On the other hand, others believe that heteropolar bonds are always preferred (**chemically ordered covalent network** or the **COCN** model). In this second case, only A–B bonds exist in the stoichiometric crystalline compound (which presumably carry into the glass). On the A-rich

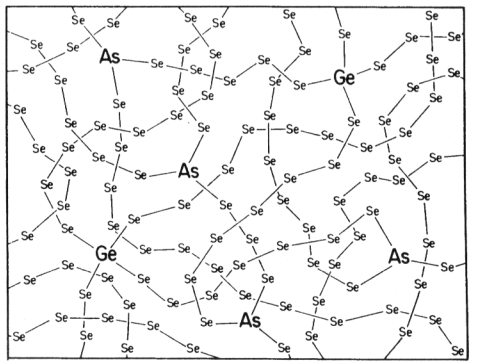


**Figure 5-42.** 2-D representation of the bonding in Ge–As–Se glass. Note crosslinking of linear chains by As (3-coordination) and Ge (4-coordination). (After R. Zallen, *The Physics of Amorphous Solids*, Fig. 3.7, p. 98. Wiley & Sons, New York, 1983. Reproduced with permission of the publishers.)

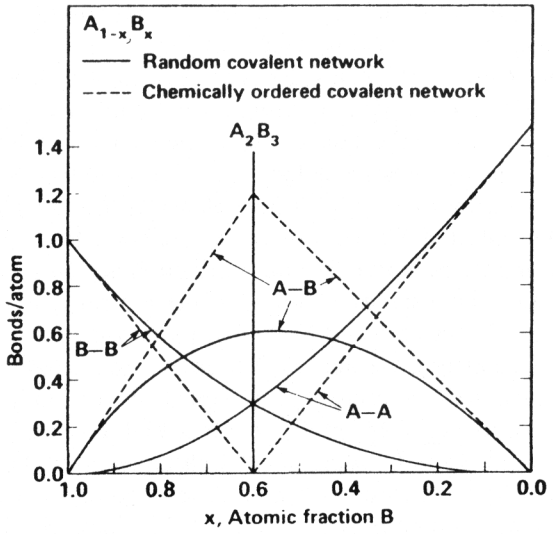


**Figure 5-43.** Bond statistics in (a) a 3:2 network (e.g., $As_2Se_3$), and (b) a 4:2 network (e.g., $SiO_2$). (After Lucovsky and Hayes [33]. Reproduced with permission of Springer-Verlag.)

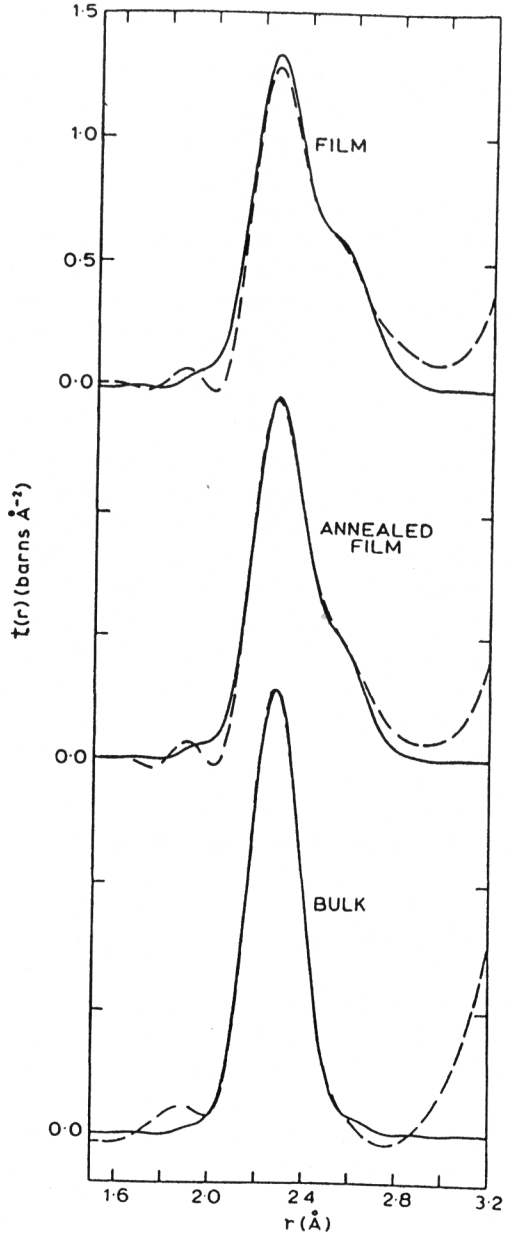


**Figure 5-44.** Neutron total correlation function for As–S films and bulk. The bulk sample only has one type of bond, presumably heteropolar. This peak clearly has a shoulder in the film indicating the presence, perhaps, of the homopolar ("wrong" type) of bond. (After Daniel *et al.* [34]. Reproduced with permission of Elsevier Science Publishers.)

side of the stoichiometric compound, only A–A and A–B bonds exist, whereas on the B-rich side only B–B and A–B bonds exist. The bond statistics for these two different models are shown [33] for a compound such as $Sb_2Se_3$ in Fig. 5-43. The characters of the different structural groups present would then dictate the properties of the glasses.

There is some evidence that different preparation techniques may lead to different short- and medium-range order. An example [34] of this is shown in Fig. 5-44, where the neutron diffraction-derived total correlation function, $t(r)$, of As–S films prepared by bulk melting appears to have only one type of bond distance (presumably the heteropolar bond), whereas the vapor-deposited material has two distinct sets of bond lengths (which do not change even upon annealing).

Chalcohalides are formed [35] by melting together the chalcogen elements (Te, Se, and S), halogens, and other group II–IV elements. The glass-forming range is very wide. Compositions such as $Te_3Cl_2$, $Te_3Br_2Se$, and $Te_4I_5S$ are typical of this family (also called "TeX" glasses). Chalcohalides are of considerable interest because of their greater transparency in the IR relative to the chalcogenides. In the chalcohalides, the halogens require only one-coordination, and hence act as chain-ending units. As a result, the fluidity of the structure at comparable temperatures greatly increases in comparison to the corresponding chalcogenides. The $T_g$'s of most chalcohalides are in the 60–160°C range.

## 5.16. Heavy Metal Fluoride Glasses (HMFG)

Suggested reading: M. Drexhage, *Treatise on Mat. Sci. & Tech.*, Vol. 26, *Glass IV* (M. Tomozawa and R. H. Doremus, eds.), pp. 151–243 (1985).

The bonding in the oxide structures is known to be partly ionic and partly covalent. On the other hand, the HMFG are made up of non-oxide ionic salts. The covalency content in these glasses is quite small.

Glass formation in the HMFG system was discovered only as recently as 1974 at the University of Rennes, France. However, because of their possible use as a fiber material for long-distance telecommunication, a vast amount of research effort has been poured into the study of HMFG glasses. The glass formation range is very wide—virtually any metal fluoride can be incorporated into the structure. It is now known that, in addition to the fluorides, other halides can also be included in a wide range of glasses. HMFG compositions are divided into two classes: those based on $ZrF_4$ or $HfF_4$ as glass formers, and those excluding $ZrF_4$ or $HfF_4$. In the former category, called fluorozirconates or fluorohafnates, the glasses generally have



**Table 5-6.** Heavy Metal Fluoride Glass Systems and Some of Their Properties

| Composition (mole %) | Acronym | $T_g$ (°C) | $T_x$ (°C) | Density (gm/cm$^3$) | $n_D$ |
|---|---|---|---|---|---|
| $64ZrF_4$–$36BaF_2$ | ZB | 300 | 352 | 4.66 | 1.522 |
| $53ZrF_4$–$47ThF_4$ | ZT | 490 | 572 | 5.72 | 1.551 |
| $50ZrF_4$–$25BaF_2$–$25NaF$ | ZBN | 240 | 300 | 4.50 | 1.50 |
| $63ZrF_4$–$33BaF_2$–$4GdF_3$ | ZBG | 310 | 390 | — | 1.529 |
| $62ZrF_4$–$33BaF_2$–$5LaF_3$ | ZBL | 306 | 380 | 4.79 | 1.523 |
| $62HfF_4$–$33BaF_2$–$5LaF_3$ | HBL | 312 | 395 | 5.78 | 1.514 |
| $57.5ZrF_4$–$33.75BaF_2$–$8.75ThF_4$ | ZBT | 320 | 400 | 4.80 | 1.523 |
| $57.5HfF_4$–$33.75BaF_2$–$8.75ThF_4$ | HBT | 319 | 396 | 6.19 | — |
| $56ZrF_4$–$15BaF_2$–$6LaF_3$–$4AlF_3$–$20NaF$ | ZBLAN | 275 | 405 | 4.27 | 1.499 |
| $55ZrF_4$–$30BaF_2$–$15UF_4$ | ZBU | 320 | 400 | 5.01 | — |
| $50ZrF_4$–$43ThF_4$–$7YF_3$ | ZTY | 465 | 559 | 5.41 | 1.537 |
| $45ZrF_4$–$36BaF_2$–$11YF_3$–$8AlF_3$ | ZBYA | 344 | 425 | 4.54 | 1.507 |
| $57ZrF_4$–$36BaF_2$–$3LaF_3$–$4AlF_3$ | ZBLA | 310 | 390 | 4.61 | 1.516 |
| $57HfF_4$–$36BaF_2$–$3LaF_3$–$4AlF_3$ | HBLA | 312 | 400 | 5.88 | 1.504 |

50–70% $ZrF_4$ or $HfF_4$, although compositions containing as little as about 30 mol % can form glasses. The primary network modifier in these glasses is generally $BaF_2$ in amounts of about 30 mol %. In the second category, the glasses include large amounts of $BaF_2$, $ThF_4$, $AlF_3$, and $ZnF_2$. Selected glass compositions of interest and their physical properties (glass transition temperature $T_g$, crystallization temperature $T_x$, density, and refractive index) are listed in Table 5-6. Glasses are often called by their acronyms: for instance, glass $53ZrF_4{\cdot}20BaF_2{\cdot}4LaF_3{\cdot}3AlF_3{\cdot}20NaF$ is called "ZBLAN."

Because of the multicomponent nature of these glasses, structural studies have been very difficult. The interpretation of x-ray scattering experiments has often been accomplished using complementary techniques such as molecular dynamics [36]. For the simplest binary system, $ZrF_4$–$BaF_2$, the schematics of the glass structure are shown in Fig. 5-45. Unlike other glass network formers where the coordination around the NWF cation is low, the coordination of fluorine around the tetravalent Zr is 7.6 on average. The structure is made up of $ZrF_7$ and $ZrF_8$ polyhedra not only joined to each other at corners, but also sharing edges and faces. Fluorine may be of three types: the edge-bridging ("E"), the corner-bridging ("C"), and the nonbridging terminal ("T"). Polyhedral arrangements found in glasses are shown in Fig. 5-46. Some arrangements (Fig. 5-46a) are typical of those found in crystals, while others (Fig. 5-46b) are closely related. (Here, the reader may note that the HMFGs violate just about every criterion of glass formation according to Zachariasen.) The charge neutrality of the polyhedra is observed by "modifying" cations, such as $Ba^{2+}$, occupying the interstitial spaces. The

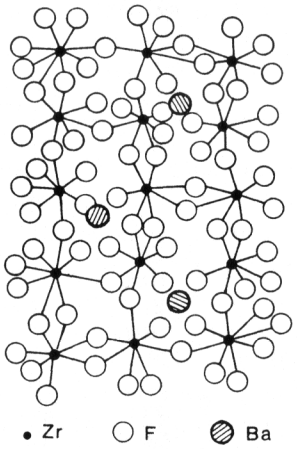


**Figure 5-45.** MD simulation of $67ZrF_4 \cdot 33BaF_2$ glass. (After Phifer and Angell [36]. Reproduced with permission of Elsevier Science Publishers.)

primary network forming Zr–F bonds in these glasses are believed to be mostly ionic, as opposed to roughly 50–50 ionic and covalent as in $SiO_2$ and $B_2O_3$ (see Stanworth's electronegativity criterion for glass formation [22].

In those glasses where $AlF_3$ is present in large quantities, MD simulations suggest that Al is present as $AlF_6$ octahedra sharing corners and making a complex network in which Ba, Ca, etc., occupy the interstitial positions. The coordination of fluorine around Ba is found to be between 8 and 9. Interestingly enough, the densities of some of these glasses are higher than those of the corresponding composition crystals [38] (see Section 2.2).

Baldwin and Mackenzie [39] have attempted to classify fluoride glass network formers and modifiers in a manner similar to that for the oxide glasses by Sun (see Section 3.1.2). The dissociation energy of the molecule $MF_x$ was divided by the expected coordination number to obtain value for the $B_{M-F}$ (single M–F bond strength), and classified according to whether or not the bond strength was sufficiently high to discourage crystalline rearrangements. Like the oxides, those elements whose single bond strength with F exceeds about 80 kcal/mol ($\sim 335\ kJ \cdot mol^{-1}$) are classified NWF, those less than 60 kcal/mol are NWM, and the ones between 60 and 80 kcal/mol are the intermediates. Mackenzie [40] later incorporated Rawson's criterion (Section 3.1.2) of dividing $B_{M-F}$ by the melting temperature of the compound $MF_x$ to assess whether the available energy was sufficient to break the bonds. The concepts so generated were used to examine glass formation in the presence of other halogen ions.

Poulain [41] suggested that glass formation in the HMFG systems would



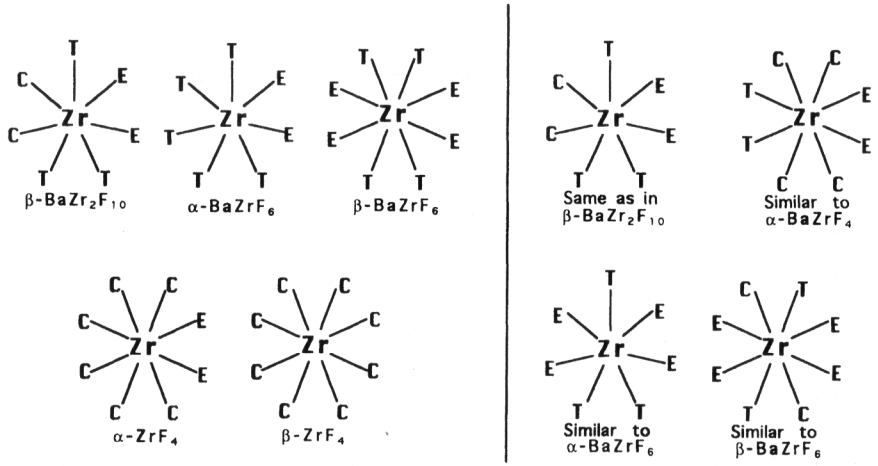


**Figure 5-46.** Proposed Zr-F polyhedra with $F^-$ characterized as E (edge-bridging), C (corner-bridging), and T (terminal or nonbridging). (a) Polyhedra that may occur in glass and are as found in fluorozirconate crystals. (b) Additional types that may occur in glass and are similar to those found in crystals. (After Phifer and Angell [36]. Reproduced with permission of Elsevier Science Publishers.)

occur if the anionic distribution in the glass is such that the number of potential cationic sites exceeds the available number of cations. This can be possible for high-field-strength cations that, by virtue of having a small ionic radius, can be fitted into a large number of possible sites. However, large repulsion from extremely high-field-strength cations could lead to the disappearance of the ionic bond. Poulain used the ratio of the cationic to anionic field strengths, $F_c/F_a$, as a parameter to determine glassforming capability. It appears that glass network former cations were those for which $10.5 > F_c/F_a > 2.5$. (The limits were established empirically.) Large-radius cations such as $Ba^{2+}$ and $La^{3+}$ tended to stabilize the structure by precluding highly ordered anionic close packing.

## Exercises

**1.** What is the representative formula for the following glass network?

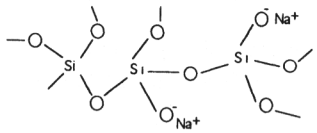

Answer: There are three silicons, two sodiums, two nonbridging oxygens, counted full, two bridging oxygens (shared between tetrahedra shown), counted full, and six bridging oxygens (including missing oxygen on lower left) shared between tetrahedra (not shown), counted halves. Thus, the formula ought to be $Na_2Si_3O_7$ or $Na_2O{\cdot}3SiO_2$.

**2.** Convert the following to wt. %:
(a) $15Na_2O{\cdot}10CaO{\cdot}75SiO_2$ (mol %)

[Answer: $15.53Na_2O{\cdot}9.35CaO{\cdot}75.12SiO_2$]

(b) $Na_2O{\cdot}2B_2O_3{\cdot}6SiO_2$

[Answer: $11.05Na_2O{\cdot}24.8B_2O_3{\cdot}64.15SiO_2$]

**3.** Convert the following wt. % composition to mol %:
$14BaO{\cdot}10CaO{\cdot}14Al_2O_3{\cdot}62SiO_2$

[Answer: $6.34BaO{\cdot}12.4CaO{\cdot}19.53Al_2O_3{\cdot}71.73SiO_2$]

**4.** A glass tank usually melts $15Na_2O{\cdot}10CaO{\cdot}75SiO_2$ (wt. %) continuously using $NaCO_3$, $CaCO_3$, sand, and 25% cullet (broken glass of the same composition) as raw materials. An engineer by mistake happened to mix 1,000 kg of the batch on a 15–10– 75 mol % basis. Calculate the shortest corrective action (one raw material additive).

**5.** Calculate the $f_{NBO}$ and $Y$ from first principles in a $45Na_2O{\cdot}55SiO_2$ (mol %) glass. Compare your results of $Y$ with $Q_n$ shown in Fig. 5-14. Sketch a representative structure of this glass.

**6.** Calculate the $f_{NBO}$ and $Y$ from first principles in a $15K_2O{\cdot}10SrO{\cdot}\ 75SiO_2$ (mol %) glass.

**7.** Calculate the $f_{NBO}$ in a fused silica specimen containing 2 ppm $Na_2O$ and 10 ppm $Al_2O_3$ impurity. Assume that none of the Na ions are associated with the Al. (Answer: 32 ppm.)

**8.** Assume that $AlPO_4$ can form a glass isomorphic to fused silica. Sketch the expected RDF if, for simplicity, the ionic radii are assumed to be $Al^{3+} = 0.06$ nm, $P^{5+} = 0.03$ nm, and $O^{2-} = 0.12$ nm. Sketch a representative structure of this glass.

**9.** Calculate the average chain length for Se chains having chain ending units such that the average coordination number is 1.66.



## References


1. R. L. Mozzi and B. E. Warren, *J. Appl. Cryst.* **2**, 164 (1969).
2. R. J. Bell and P. Dean, *Nature (London)* **212**, 1354–1356 (1966).
3. D. L. Evans and S. V. King, *Nature (London)* **212**, 1353–1354 (1966).
4. T. F. Soules, in *Glass Science and Technology* (D. R. Uhlmann and N. J. Kreidl, eds.), Vol. 4a, pp. 267–388. Academic Press, New York, 1990.
5. F. Wooten and D. Weaire, *Solid State Phys.* **40**, 1–42 (1987).
6. S. C. Cherukuri, "Structural Studies of Vitreous Silica and Cristobalite," Ph.D. thesis, Alfred University, 1983.
7. F. Stillinger and T. Weber, *Phys. Rev.* **B31**, 5262 (1985).
8. R. L. Mozzi and B. E. Warren, *J. Appl. Cryst.* **3**, 2512 (1970).
9. T. F. Soules and A. K. Varshneya, *J. Am. Ceram. Soc.* **64**(3), 145–150 (1981).

10a. R. Dupree, D. Holland, P. W. McMillan, and R. F. Pettifer, *J. Non-cryst. Sol.* **68**(2–3), 399–410 (1984).

10b. H. Maekawa, T. Maekawa, K. Kawamura, and T. Yokokawa, *J. Non-cryst. Sol.* **127**, 53–64 (1991).

10c. S. R. Elliott, *J. Non-cryst. Sol.* **123**, 149–164 (1990).

11. A. Dietzel, *Sprechsaal* **62**, 506 (1929).
12. E. J. Gooding and W. E. S. Turner, *J. Soc. Glass Tech.* **18**, 32T (1934).
13. J. Biscoe and B. E. Warren, *J. Am. Ceram. Soc.* **21**, 287 (1938).
14. B. E. Warren, *J. Appl. Phys.* **13**, 602 (1942).
15. P. J. Bray and J. G. O'Keefe, *Phys. Chem. Glasses* **4**, 37–46 (1963).
16. C. M. Kuppinger and J. E. Shelby, *J. Am. Ceram. Soc.* **68**(9), 463 (1985).
17. P. K. Gupta, *Proc. Intl. Cong. on Glass, XIV New Delhi, Part I*, pp. 1–10, 1986.
18. M. E. Milberg, J. G. O'Keefe, R. A. Verhelst, and H. O. Hooper, *Phys. Chem. Glasses* **13**(3), 79–84 (1972).
19. E. D. Lacy, *Phys. Chem. Glasses* **4**(6), 234–238 (1963).
20. J. O. Isard, *J. Soc. Glass. Technol.* **43**, 113–123T (1959).
21. G. J. Bair, *J. Am. Ceram. Soc.* **13**, Part I, 339–347 and Part II, 347–358 (1936).
22. M. F. Mydlar, N. J. Kreidl, J. K. Hendren, and G. T. Clayton, *Phys. Chem. Glasses*, **11**(6), 196–204 (1970).
23. A. E. R. Westman, in *Modern Aspects of the Vitreous State*, Vol. 1 (J. D. Mackenzie, ed.), pp. 63–91. Butterworths, London, 1960.
24. A. K. Varshneya, R. F. Busbey, and T. F. Soules, *J. Non-cryst. Sol.* **69**, 381–385 (1985).

25. K. Kamiya and S. Sakka, *Phys. Chem. Glasses* **20**(3), 60 (1979).
26. D. E. Polk, *J. Non-cryst. Sol.* **5**, 365 (1971).
27. S. C. Moss and J. F. Graczyk, *Phys. Rev. Lett.* **23**, 1167 (1969).
28. P. Steinhardt, R. Alben, and D. Weaire, *J. Non-cryst. Sol.* **15**, 199 (1974).
29. J. D. Bernal, *Nature (London)* **183**, 141 (1959); *Proc. Roy. Soc. (London)* **A280**, 299 (1964).
30. J. L. Finney, *Proc. Roy. Soc. (London)* **A319**, 479 (1970).
31. C. H. Bennett, *J. Appl. Phys.* **43**, 2727 (1972).
32. See S. R. Elliott, *Physics of Amorphous Solids*, 2nd Ed., p. 154. Longman Scientific and Technical, Harlow, Essex, 1990.
32b. P. H. Gaskell, *Nature (London)* **289**, 474 (1981).
33. G. Lucovsky and T. M. Hayes, in *Amorphous Semiconductors* (M. H. Brodsky, ed.), p. 215. Springer-Verlag, Berlin, 1979.
34. M. F. Daniel, A. J. Leadbetter, A. C. Wright, and R. N. Sinclair, *J. Non-cryst. Sol.* **32**, 271–293 (1979).
35. J. Lucas and X. H. Zhang, *J. Non-cryst. Sol.* **125**, 1–16 (1990).
36. C. C. Phifer and C. A. Angell, *J. Non-cryst. Sol.* **94**, 315–335 (1987).
37. See H. Rawson, *Inorganic Glass-Forming Systems*, p. 20. Academic Press, London, 1967.
38. T. Tanba, H. Inoue, Y. Arai, H. Hasegawa, M. Misawa, and I. Yasui, *Proc. Vth Intl. Symp. on Halide Glasses, Shizuko, Japan*, pp. 293–298. (1988).
39. C. M. Baldwin and J. D. Mackenzie, *J. Am. Ceram. Soc.* **62**, 537 (1979).
40. J. D. Mackenzie, Paper 26 at the 2nd Int. Symp. on Halide Glasses, Rensselaer Polytechnic Inst., Troy, New York, 1983.
41. M. Poulain, *Nature (London)* **293**, 279 (1982).

## Chapter 6

# Composition–Structure–Property Relationship Principles

So far we have studied the range of glass compositions and how the compositions affect the structure. The properties of a substance are controlled by the structure — how the various atoms are organized (or disorganized) to make up the particular substance. This is the chapter where we shall make a gradual transition in the form of basic principles to understanding glass properties — to examine the interrelationship of composition, structure, and properties. The details of specific property variations are saved for specific chapters later.

### 6.1. General Principles

In the previous chapters, we have emphasized one particular aspect of the glass structure: the lack of long-range periodicity in the arrangement of atoms. Whether the bonding is ionic, covalent, van der Waals, metallic, or a mixture of these, this "*more-or-less randomness*" is the most important feature of a glass. Such an arrangement of atoms in general gives rise to slightly more open packing than that found in the corresponding crystal (although there are exceptions). It follows that whereas small displacements of atoms from their regular periodic locations in a crystal might be higher-energy positions called "defects," the use of such a word in glass leads to